Research Square

Preprints are preliminary reports that have not undergone peer review.
They should not be considered conclusive, used to inform clinical practice,
or referenced by the media as validated information.

Aeromagnetic and gravity interpretation of basement structure, basin configuration and mineral–hydrocarbon prospectivity in the Okigwe–Afikpo area (sheets 312 and 313), Lower Benue Trough, south-eastern Nigeria

cyril Chibueze okpoli

cyril.okpoli@aaua.edu.ng

Adekunle Ajasin University

olumide fashola

University of Ibadan

Article

Keywords: Aeromagnetic data, Bouguer gravity, Euler deconvolution, Lower Benue Trough, Anambra Basin, Structural lineaments

Posted Date: November 25th, 2026

DOI: https://doi.org/10.21203/rs.3.rs-11316210/v1

License: This work is licensed under a Creative Commons Attribution 4.0 International License.
Read Full License

Additional Declarations: No competing interests reported.

Aeromagnetic and gravity interpretation of basement structure, basin configuration and mineral–hydrocarbon prospectivity in the Okigwe–Afikpo area (sheets 312 and 313), Lower Benue Trough, south-eastern Nigeria

Cyril Chibueze Okpoli[1], Fashola Olumide[2]

1.Department of Earth Sciences, Faculty of Science, Adekunle Ajasin University, PMB 001, Akungba-Akoko, Ondo State, Nigeria

2. Department of Geology, University of Ibadan, Ibadan, Nigeria

Corresponding author: cyril.okpoli@aaua.edu.ng

ORCID: 0000-0001-8336-0658

Abstract

The Okigwe–Afikpo area (NGSA sheets 312 and 313) lies on the south-western flank of the Abakaliki Anticlinorium in the Lower Benue Trough. Earlier geophysical work there relied largely on aeromagnetic data and gave little attention to structure or to mineral and hydrocarbon prospectivity. This study combines high-resolution aeromagnetic data with a Bouguer gravity grid to describe basement structure and basin configuration at reconnaissance scale. Both datasets were processed in Oasis montaj. The magnetic grid was reduced to the equator and enhanced by regional–residual separation, upward and downward continuation, directional and total horizontal derivatives, the tilt derivative, the analytic signal and the second vertical derivative. The gravity grid received comparable treatment. Depths came from Euler deconvolution, radially averaged power spectra and two-dimensional forward models. The reduced-to-equator anomaly ranges from −21.8 to 188.2 nT and the Bouguer anomaly from 7.8 to 57.6 mGal. Magnetic lineaments trend mainly NE–SW, with a subordinate E–W set, whereas gravity gradients trend mainly NW–SE and N–S. Magnetic Euler solutions lie between about 296 and 3,265 m, spectral analysis gives deeper sources at 1.7–2.0 km and shallower sources above 0.4 km, and gravity Euler solutions reach more than 2,000 m. Two preliminary profile models place the top of the basement at about 0.1–0.2 km beneath a central high and at more than 1.2–2 km towards the profile ends. The results point to a fault-segmented basin that hosts shallow intrusive bodies. Potential-field data cannot establish source-rock quality, thermal maturity or mineralisation, so the zones identified here are targets for seismic, geochemical and drilling follow-up rather than demonstrated prospects.

Keywords Aeromagnetic data · Bouguer gravity · Euler deconvolution · Lower Benue Trough · Anambra Basin · Structural lineaments

1 Introduction

Airborne magnetic surveys map lateral changes in rock magnetisation, which in turn reflect the distribution of magnetite-bearing rocks, structural breaks and the depth to magnetic basement (Telford et al. 1990; Reeves 2005). Gravity surveys respond instead to density contrasts, and they therefore sample a different physical property of the same crust (Hinze et al. 2013). Used together, the two methods offer a cheap and fast way to cover large areas and to separate features that either method alone would leave ambiguous. This is particularly useful in sedimentary terrains such as the Benue Trough, where outcrop is patchy and deep drilling is sparse.

Magnetic data are more widely used than gravity data in mineral exploration. A principal reason is that magnetic data are recorded quickly from the air, often together with radiometric and electromagnetic data, whereas gravity surveys on the ground demand more time and logistics (Hinze et al. 2013). Faults and fractures that control fluid movement can be traced from magnetic and gravity lineaments, and this holds whether the target is a hydrocarbon trap or a mineralised structure. Magnetic interpretation is nevertheless complicated by the dipolar geometry of the field, by remanent as well as induced magnetisation, and by the low inclination found near the magnetic equator, where simple reduction to the pole becomes unstable (MacLeod et al. 1993). Gravity interpretation, for its part, depends on the reduction density and on how the regional field is removed.

The Lower Benue Trough is regarded as a frontier province with both hydrocarbon and solid-mineral potential, and most published geophysical work on it is magnetic. In the Okigwe–Afikpo sector, Ugwu et al. (2013) used forward and inverse modelling of aeromagnetic data and obtained depths of 3.0–12.7 km for buried anomalous bodies. Ofoegbu and Onuoha (1991) found two source depths over the Abakaliki Anticlinorium, with the deeper sources at 1.2–2.5 km. Igwesi and Umego (2013) reported two-layer spectral depths in parts of the Lower Benue Trough, and Oha et al. (2016) showed that shallow intrusions dominate the magnetic response of the southern Benue Trough: at least 40% of the basin contains magmatic bodies shallower than 200 m, and Euler and source-parameter-imaging depths average only 0.42 and 0.37 km. Abdullahi and Kumar (2021) combined three magnetic depth methods with a two-dimensional gravity model and obtained basement depths of 3.8–8.5 km for the Afikpo Basin, 3.1–9.8 km for the Abakaliki Anticlinorium and 8.4–9.1 km for the Anambra Basin. More recently, Osinowo and Taiwo (2020) delineated sections of the basin with sedimentary thickness greater than 3 km, and Ijeh et al. (2025) estimated deeper magnetic sources at an average of about 2.5 km beneath the Okigwe sheet. Okoli et al. (2024) mapped NE–SW, NW–SE and NNW–SSE to E–W fracture sets from tilt-derivative maps over a block that includes the Afikpo sheet. Studies that integrate gravity with magnetic data are fewer (Abdullahi et al. 2019, 2023; Yenne et al. 2025).

These estimates differ widely. Part of the spread is real structural variation, but much of it arises because the studies estimate different quantities: the tops of intrusive bodies, ensembles of magnetic sources, or the sediment–basement interface. Few of them compare magnetic and gravity results for the same

ground, and even fewer treat the Okigwe and Afikpo sheets together using gridded data that were processed consistently.

Solid minerals are another reason for attention. Nigeria's solid-minerals sector contributed about 0.83% of gross domestic product in 2022 and 0.75% in 2023 (NEITI 2024), and national mineral output comes from private companies and from artisanal and small-scale miners (USGS n.d.). The Nigeria Extractive Industries Transparency Initiative (NEITI) describes the sector's potential as largely untapped (NEITI 2024), so there is a continuing push to document the country's mineral endowment as part of the effort to diversify the economy away from oil and gas. Ironstone mineralisation and extensive quarrying are conspicuous around Okigwe, and Pb–Zn(–Cu) mineralisation is documented elsewhere in the Lower Benue Trough (Olade and Morton 1985; Akande and Mücke 1993). Structural corridors identified from potential-field data are therefore of interest to mineral and groundwater exploration as well as to petroleum geology.

This study aims to delineate the structural features of the Okigwe–Afikpo area from aeromagnetic and gravity data (sheets 312 and 313) and to infer how these structures influence basin configuration. The specific objectives are to (1) describe and interpret variations in the magnetic and gravity anomalies in terms of magnetisation and density contrast; (2) estimate the thickness of sedimentary cover, and hence the depth to magnetic basement, from the magnetic data and compare it with gravity-derived depths; and (3) relate the regional geology to the structural trends that emerge.

2 Study area and geological setting

2.1 Location, climate, topography and drainage

The study area covers the Okigwe (sheet 312) and Afikpo (sheet 313) 1:100,000 sheets in the Lower Benue Trough and the Anambra Basin of south-eastern Nigeria (Fig. 1). The two half-degree sheets lie between about 7°00′ and 8°00′ E and 5°30′ and 6°00′ N, a block of roughly 110 km by 55 km (about 6,100 km²) that includes the towns of Okigwe and Afikpo.

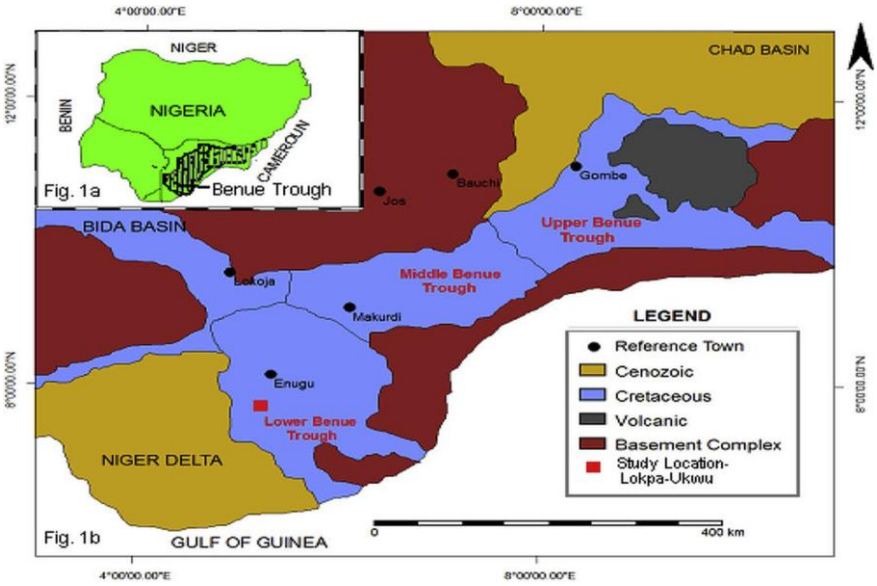

Fig. 1 Geological map of the Lower Benue Trough (adapted from Olade 1975)

The climate is humid tropical, with a wet season and a drier season and warm temperatures all year. At Okigwe the temperature typically ranges from about 18 to 31 °C and rarely falls below 14 °C or exceeds 32 °C; at Afikpo it typically ranges from about 19 to 31 °C and rarely falls below 16 °C or exceeds 33 °C (Weather Spark n.d.).

The terrain around Okigwe is hilly and undulating compared with the low-lying relief of the rest of Imo State. A few hilltops reach about 300 m, and the average crest height lies between 120 and 180 m above sea level. The Afikpo area is underlain largely by shale and clay, which weather to fertile soils and supply material for mud-brick building. The area is drained by streams of the Cross River system and by the Ebonyi (Asu) River. Streams emerge from the ridges and run onto plains that widen at the foot of the ridges, and the pattern is mainly dendritic with local rectangular or trellis segments. Lithology influences stream density and development, and the streams have not yet reached maturity. Springs and seepages are common and supply some villages with water.

2.2 Regional tectonic setting

The Benue Trough is a NE–SW-trending Cretaceous rift basin about 1,000 km long, which extends from the northern margin of the Niger Delta to the Chad Basin. It is generally regarded as the failed arm of a triple junction associated with the separation of Africa and South America (Grant 1971; Burke et al. 1972; Olade 1975). Benkhelil (1989) argued instead for a model dominated by transcurrent movement along Atlantic transform faults, in which the trough behaved as a complex pull-apart structure. That view accounts for the structural patterns that simple orthogonal extension does not explain, and it is consistent with the alkaline magmatism of the trough and with the compressional phase of the Santonian (Benkhelil and Robineau 1983). Hoque and Nwajide (1984) and Reijers and Nwajide (1998) provide further accounts of its evolution.

The trough is divided into the Upper, Middle and Lower Benue Trough. The Lower Benue Trough comprises the Abakaliki Anticlinorium, the Anambra Basin, the Afikpo Syncline (or Synclinorium), the Mamfe Rift and the Calabar Flank (Hoque and Nwajide 1984; Benkhelil 1989). Santonian compression folded and uplifted the Aptian–Coniacian fill to form the Abakaliki Anticlinorium, with the Asu River Group in its core and the Eze-Aku Group on its flanks. Subsidence on either side of the fold belt produced the Anambra Basin to the west and the Afikpo Syncline to the east and south-east (Murat 1972; Whiteman 1982; Benkhelil 1989). The study area occupies the south-western flank of the Abakaliki Fold Belt, between the Anambra Basin and the Afikpo Syncline (Fig. 2). Brittle structures in the Afikpo Basin record a later, terminal-Cretaceous extensional regime (Odigi and Amajor 2009).

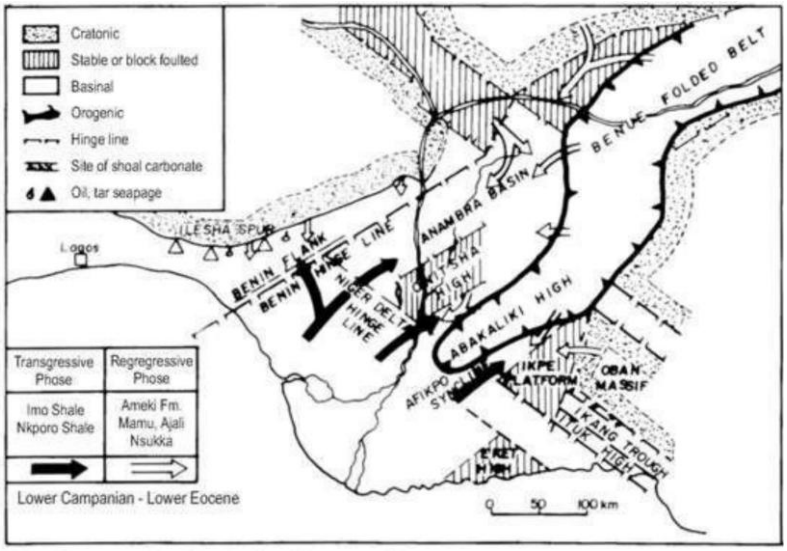

Fig. 2 Tectonic map of south-eastern Nigeria showing the Anambra Basin (adapted from Murat 1972)

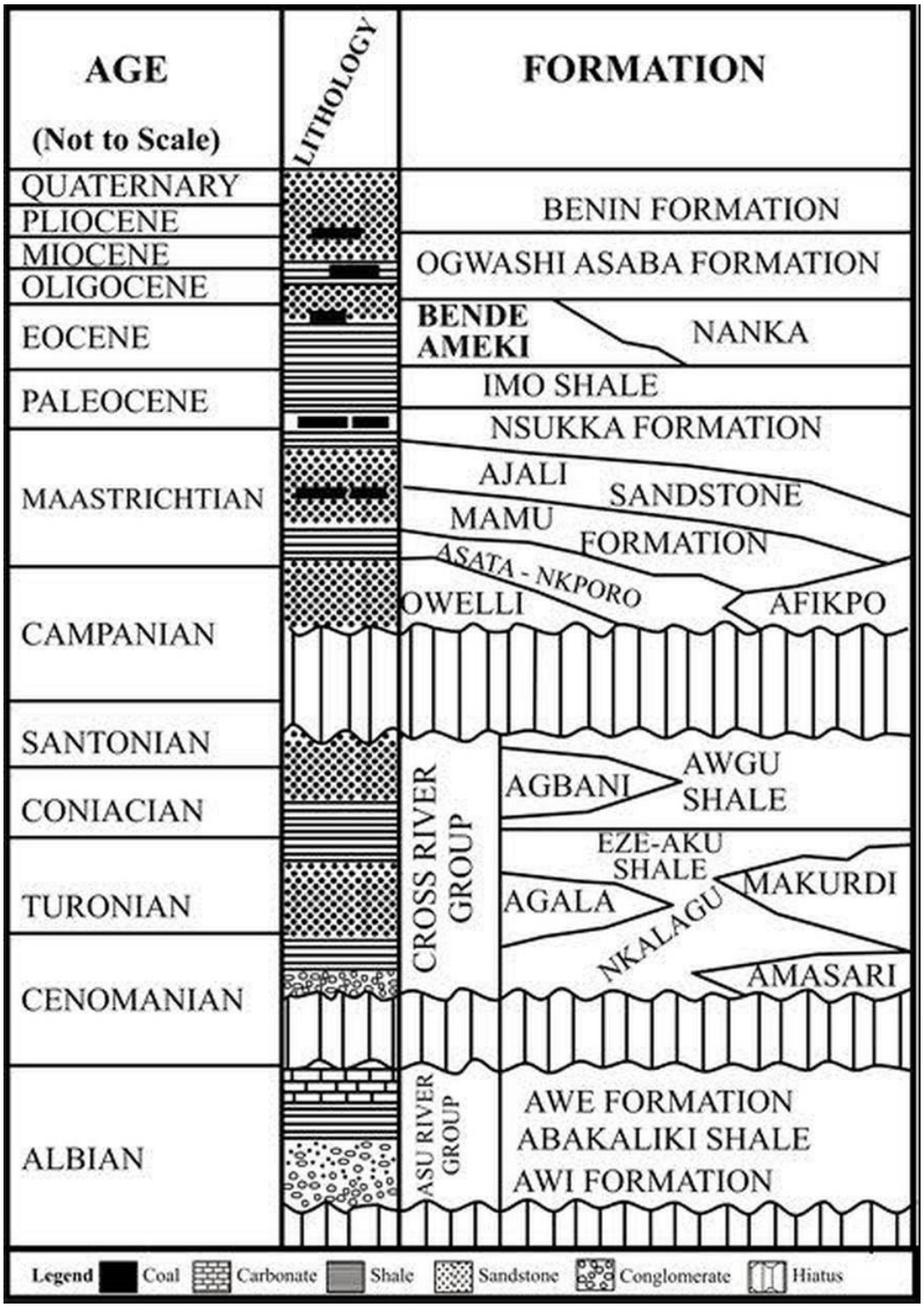

Fig. 3 Stratigraphy of the Lower Benue Trough (Whiteman 1982)

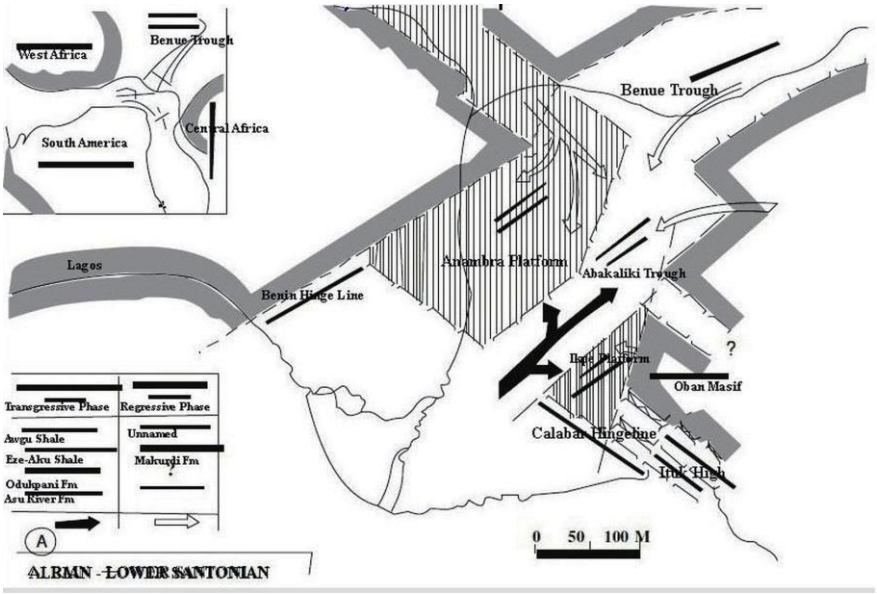

Fig. 4 Tectonic map of south-eastern Nigeria from the Albian to the Tertiary (adapted from Murat 1972)

2.3 Stratigraphy

Sedimentation began in the Aptian to early Albian with fluvial and lacustrine arkosic sandstones and shales (the Bima Sandstone in the north and the Mamfe Formation in the south). Two transgressive–regressive cycles followed between the middle Albian and the Coniacian and filled the southern trough with mudrocks, sandstones and limestones, to a thickness estimated at about 3,500 m (Murat 1972; Hoque and Nwajide 1984; Olade 1975). These sediments belong to the Albian Asu River Group, the Cenomanian Odukpani Group, the Turonian Eze-Aku Group and the Coniacian Awgu Formation (Figs. 3 and 4).

The Asu River Group rests unconformably on Precambrian basement, which consists of granitic and migmatitic rocks. It has an estimated thickness of 2,000 m in the Abakaliki–Afikpo basins and an Albian to Cenomanian age (Ofoegbu 1985). It comprises argillaceous sandy shales, laminated and micaceous sandstones and minor limestones, with interfingering mafic volcanics (Nwachukwu 1972). The overlying Turonian Eze-Aku Shale is nearly 1,000 m thick and consists of calcareous flaggy shales and siltstones with thin sandy and shaly limestones and calcareous sandstones (Reyment 1965). In the Afikpo Basin its sandy facies form the Amasiri Sandstone. Folded Eze-Aku Shale and Asu River Group are exposed from about 8 km north-east of Okigwe, where they are overlain unconformably by the Nkporo Shale.

The Anambra Basin began to form after the Santonian deformation. Its fill starts with the Campanian–Maastrichtian marine and paralic shales of the Nkporo Group, which includes the Nkporo and Enugu shales, and continues with the coal-bearing Mamu Formation and the Ajali Sandstone (Nwajide 2005; Reijers and Nwajide 1998). The Ajali Sandstone marks the peak of the regression of the Nkporo cycle, and its tidal sand waves reflect sedimentation controlled by converging littoral drift cells (Nwajide 2013). The Paleocene Nsukka Formation and Imo Shale follow, overlain by the Eocene Ameki Group

and its Nanka Sandstone. The Nkporo type locality is the Nkporo community in Abia State, and that of the Enugu Shale lies at Enugu (Reyment 1965). The Nkporo Group is only locally expected to reach the maturity needed for hydrocarbon expulsion (Reijers and Nwajide 1998).

2.4 Geology of the Okigwe and Afikpo sub-areas

Okigwe is of interest because of its widespread ironstone mineralisation and intensive quarrying. Palynological studies of the Leru, Uturu and Ihube sections dated the Nkporo Shale at Leru as late Campanian, the Mamu Formation at Uturu as early to middle Maastrichtian and the lower Nsukka Formation at Ihube as late Maastrichtian (Chiaghanam et al. 2012).

The geology of Afikpo reflects the Albian marine transgression, during which shale and sandstone accumulated. The Eze-Aku Formation is overlain by the Awgu Shale and underlain by the Odukpani Formation, and it contains the Amasiri and Afikpo sandstones. The two sandstones differ mainly in induration: the Afikpo Sandstone is more porous, whereas the Amasiri Sandstone has fewer pore spaces. The Eze-Aku Formation has a thickness of about 1,000 m, and the Amasiri facies passes laterally into the Afikpo Sandstone and, farther north, into the limestone at Nkalagu. The sequence is an alternation of shale and sandstone with gradational contacts. Cross-bedding, planar bedding, graded bedding, joints and fractures are the main sedimentary and brittle structures. The marked difference in altitude between the two sandstones, which belong to the same formation, suggests an angular unconformity between them. Aquifers are found mainly in coarse, weakly cemented sandstones and in fractured limestone with solution cavities (Ukaegbu and Akpabio 2009). Erosion and groundwater contamination are the principal hazards in the Afikpo area.

3 Data and methods

3.1 Data

The aeromagnetic data for sheets 312 and 313 were obtained from the Nigerian Geological Survey Agency (NGSA) as grid and line data at a scale of 1:100,000. They form part of the nationwide high-resolution survey flown for the NGSA by Fugro Airborne Surveys between 2003 and 2009 (Reford 2010). The survey was flown along NW–SE lines spaced 500 m apart, with tie lines at about 2 km, a mean terrain clearance of 80 m, and a magnetic sampling interval of 0.1 s (Okoli et al. 2024). The contractor corrected the data for diurnal variation and removed the International Geomagnetic Reference Field (IGRF), leaving the total magnetic intensity (TMI). Each 1:100,000 sheet covers a half-degree block of about 55 × 55 km. Processing used Geosoft Oasis montaj 6.4.2 (with the The Bouguer gravity data for the same two sheets were also obtained from the NGSA and were gridded for this study. The data are from an airborne gravity survey, flown with a gravimeter mounted on the aircraft (a stabilised-platform or strapdown system). Aircraft position and velocity came from differential GPS. Reductions comprised removal of the aircraft vertical acceleration, an Eötvös correction for the aircraft's velocity

over the rotating Earth, a latitude correction, a free-air correction to the flight height, and a Bouguer correction using 2.67 g/cm³. Terrain corrections were calculated from a digital elevation model. The data were levelled at survey crossover points and low-pass filtered to remove noise before gridding.

3.2 Processing workflow

Figure 5 summarises the workflow. The re-projected TMI grid was first filtered with a Butterworth filter to suppress near-surface noise, such as that from metallic objects, cables and variations in flight height. It was then reduced to the magnetic equator, and the regional field was removed to give the residual field. The resulting grids were used for upward and downward continuation, derivative filters, the analytic signal, lineament extraction, Euler deconvolution, spectral analysis and two-dimensional modelling. The Bouguer grid was treated in a similar way, apart from the equatorial reduction.

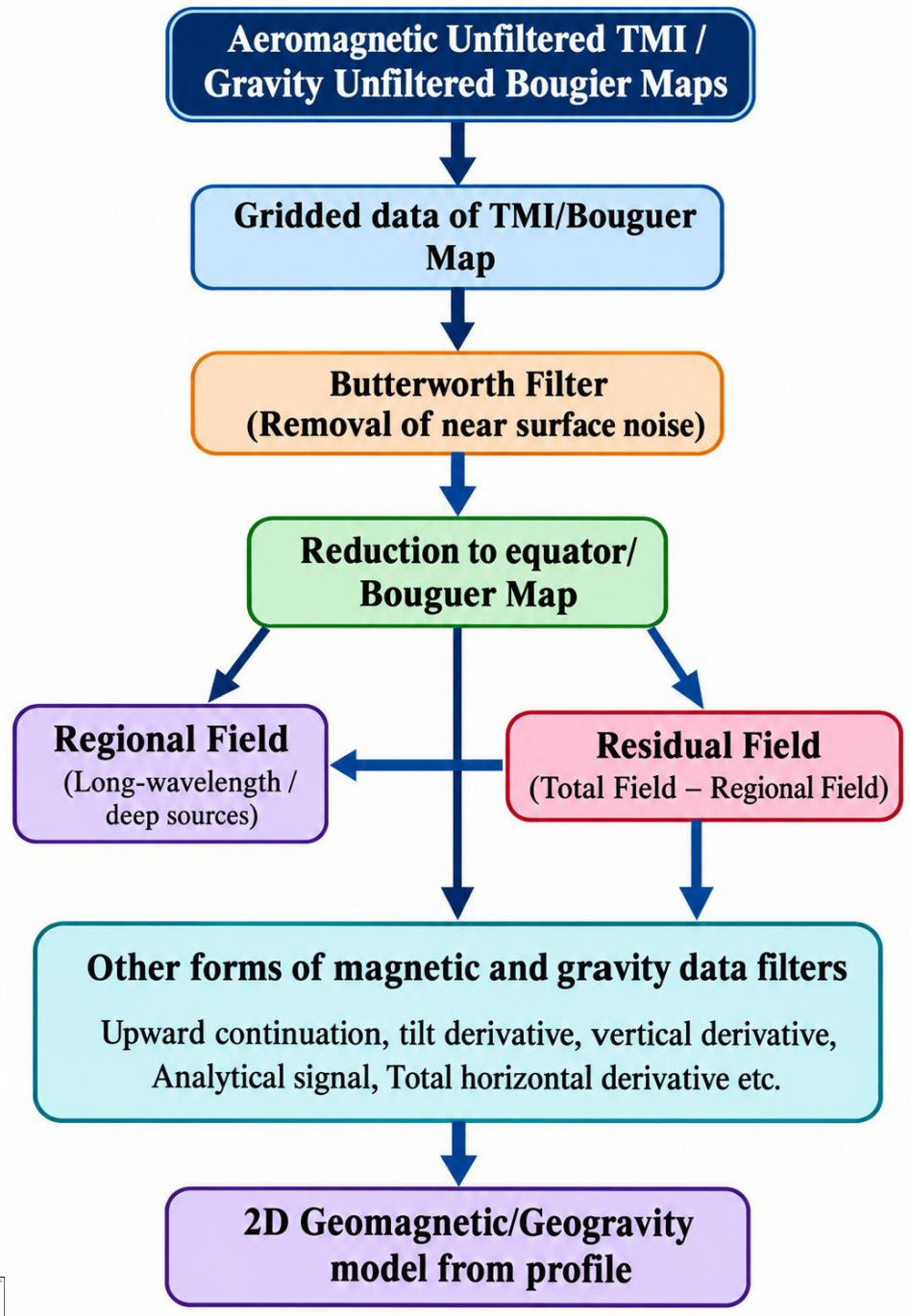

198

199 **Fig. 5** Flow chart of the data processing and interpretation workflow

200 **3.3 Magnetic processing**

201 **Reduction to the equator.** The magnetic anomaly depends on the inclination and declination of the
202 magnetisation and of the ambient field, and on the orientation of the source (Baranov 1957). At magnetic
203 latitudes below about 15°, reduction to the pole becomes unstable because the Fourier-domain operator
204 divides the spectrum by a very small term, which imposes north–south streaking on the data (MacLeod
205 et al. 1993). The study area has an inclination of about −14.5° and a declination of about −2.6°
206 (calculated from the IGRF for the centre of the area at the survey epoch; Alken et al. 2021),

corresponding to a magnetic latitude of roughly −7°. The TMI was therefore reduced to the equator (RTE), and the RTE grid served as the base for all later enhancements.

Regional–residual separation. The regional field produced by deep sources and long-wavelength anomalies was estimated by smoothing the RTE grid through upward continuation to 3 km. The residual field is the difference between the observed and regional fields:

$$\text{Residual field} = \text{RTE_TMI} - \text{Regional field} \quad (1)$$

Continuation. Upward and downward continuation recompute the field at a different level in source-free space (Henderson and Zietz 1949; Dean 1958). In the wavenumber domain the operator is

$$L(k) = e^{\pm|k|z} \quad (2)$$

where $|k| = 2\pi/\lambda$ is the wavenumber, λ is the wavelength and z is the continuation distance. The negative exponent corresponds to upward continuation, which attenuates short wavelengths and smooths the field, and the positive exponent to downward continuation, which amplifies short wavelengths and sharpens anomalies. Because downward continuation amplifies noise, it was limited to small distances (50 and 100 m). Upward continuation is regarded as a clean filter, because it produces few side effects (Pawlowski 1995), and it was applied at 200 and 500 m to emphasise deeper sources.

Derivatives. Derivative filters attenuate long-wavelength anomalies from deep sources and enhance short-wavelength anomalies from shallow ones, but they also amplify noise. First derivatives in the x, y and z directions were computed from the RTE grid. The total horizontal derivative (THD) was calculated as

$$\text{THD} = [(\partial T/\partial x)^2 + (\partial T/\partial y)^2]^{1/2} \quad (3)$$

and its maxima were used to locate faults and contacts (Verduzco et al. 2004). The tilt derivative (TDR) is the arctangent of the ratio of the vertical derivative to the THD (Miller and Singh 1994; Salem et al. 2008),

$$\text{TDR} = \tan^{-1}[(\partial T/\partial z)/\text{THD}] \quad (4)$$

and it equalises the response of strong and weak anomalies, so that the zero contour lies close to the edges of near-vertical sources. The second vertical derivative (SVD) has high resolving power and sharpens anomaly edges. The n-th order vertical derivative operator in the wavenumber domain is

$$L(k) = |k|^n \quad (5)$$

where n is the order of differentiation. Derivatives were computed in the frequency domain with the fast Fourier transform (Cooley and Tukey 1965).

Analytic signal. The amplitude of the analytic signal of the total field is obtained from the three orthogonal derivatives (Nabighian 1972; Roest et al. 1992):

$$|A(x,y)| = [(\partial T/\partial x)^2 + (\partial T/\partial y)^2 + (\partial T/\partial z)^2]^{1/2} \quad (6)$$

The analytic signal locates the edges of magnetic bodies and is largely independent of the direction of magnetisation, which is why it is useful at low magnetic latitudes, where the RTE is problematic (MacLeod et al. 1993). Its amplitude is moderately sensitive to noise and to interference between nearby sources, and where geological units are thick, depths derived from it are shallow (Al-Badani and Al-Wathaf 2017). It was computed from the RTE grid.

Lineament extraction. Lineaments were extracted automatically from the RTE grid and its derivative maps (first horizontal derivative and analytic signal), then screened manually. Edge detection used the LINE algorithm in PCI Geomatica, which applies Canny-type edge detection, thresholding, and curve extraction. The parameters were an edge-filter radius of 10 pixels, an edge-gradient threshold of 20, a minimum line-length threshold of 10 pixels, a line-fitting error threshold of 3 pixels, an angular-difference threshold of 15°, and a linking-distance threshold of 20 pixels. Extracted segments were then checked against the RTE and derivative images. Segments coinciding with flight-line noise, gridding artefacts, or cultural features such as pipelines, roads, and power lines were removed. The retained lineaments were summarised in a rose diagram of orientation (10° azimuth bins, weighted by length). They are interpreted as possible faults, contacts, or dyke-like bodies

Euler deconvolution. Euler deconvolution estimates source position and depth from the field and its gradients (Thompson 1982; Reid et al. 1990):

$$(x - x_0)\partial T/\partial x + (y - y_0)\partial T/\partial y + (z - z_0)\partial T/\partial z = N(B - T) \quad (7)$$

where (x_0, y_0, z_0) is the source position, B is the regional background and N is the structural index, which expresses the rate of decay of the field with distance from the source. The index suitable for a given anomaly can be found by seeking the value that gives the smallest perturbation in the calculated background (Barbosa et al. 1999). A structural index of 1.0 was applied to the RTE grid, which is appropriate for dyke- and sill-like sources and approximates linear contacts. The window size and a depth tolerance of 15% were selected so that the solution set contained the fewest unrealistic solutions (FitzGerald et al. 2004).

Power spectrum. The logarithm of the radially averaged power spectrum falls linearly with wavenumber, and the slope of each segment is proportional to the mean depth of the corresponding source ensemble (Spector and Grant 1970):

$$\ln P(k) = \ln C - 4\pi hk \quad (8)$$

where h is the mean depth to the top of the ensemble and k is the wavenumber in cycles per unit distance. Two segments were fitted, a low-wavenumber segment representing deeper sources and a high-wavenumber segment representing shallower ones.

Two-dimensional modelling. One profile (P-P′) was drawn across the RTE grid and modelled with the GM-SYS module of Oasis montaj, which implements the algorithms of Talwani et al. (1959) and Talwani and Heirtzler (1964). The model assumes two layers, sediments and basement. Regional-

residual separation of the gravity data used a Butterworth low-pass filter (order 8) with a cut-off wavelength of 40 km. Euler deconvolution used a structural index of 1 (contact/dyke-type sources), a 10 × 10 grid-cell window, and a depth tolerance of 10%. Depth-to-source estimates from the radially averaged power spectrum used 64 × 64 cell windows, with the slope of each spectral segment converted to depth as $h = -s/4\pi$ (s in cycles/km). Densities were set to 2.67 g/cm³ for the basement (the standard Bouguer reduction density) and 2.35 g/cm³ for the sedimentary fill, a contrast of −0.32 g/cm³. Susceptibilities were set to 0.001 SI for the sediments and 0.03 SI for the basement. The magnetic and gravity responses were fitted simultaneously by adjusting the basement geometry until the misfit between observed and calculated profiles was minimised.

3.4 Gravity processing

The Bouguer anomaly is the observed gravity minus the theoretical gravity at the station latitude, plus the free-air correction and minus the Bouguer correction, with a terrain correction where relief demands it (Telford et al. 1990; Kearey et al. 2002):

$$\Delta g_B = g_{obs} - g_{\varphi} + \Delta g_{FA} - \Delta g_{BC} \; (+ \Delta g_{TC}) \tag{9}$$

The Bouguer correction for an infinite horizontal slab of thickness h and density ρ is

$$\Delta g_{BC} = 2\pi G \rho h \approx 0.04193 \; \rho h \tag{10}$$

where Δg_{BC} is in mGal, ρ in Mg m^{-3} and h in metres. The gravity grid was subjected to the same filters as the magnetic data: downward continuation (50 and 100 m), first vertical derivative, THD, tilt derivative, analytic signal and Euler deconvolution. Gravity anomalies arise from density contrasts, which in sedimentary rocks are controlled mainly by porosity and compaction and in igneous and metamorphic rocks mainly by composition (Table 1). A two-dimensional model was constructed with GM-SYS along one profile, with sediments and basement as the two layers.

Table 1 Magnetic susceptibility and density of common rocks and minerals (after Thompson and Oldfield 1986; Telford et al. 1990; Hunt et al. 1995)

Rock or mineral	Magnetic susceptibility (SI)	Density (g cm^{-3})
Sedimentary rocks		
Shale	0.00001–0.015	1.77–3.2
Limestone	0.00031	1.93–2.90
Sandstone	0–0.020	1.61–2.76
Metamorphic rocks		
Amphibolite	0.00075	2.90–3.04
Schist	0.0003–0.003	2.39–2.9
Quartzite	0.00440	2.5–2.70
Gneiss	0.0001–0.025	2.59–3.0
Marble	0.025	2.6–2.9
Igneous rocks		
Granite	0–0.05	2.50–2.81
Diabase	0.001–0.160	2.50–3.20
Gabbro	0.001–0.090	2.70–3.50

Rock or mineral	Magnetic susceptibility (SI)	Density (g cm^{-3})
Minerals		
Graphite	0.0001	1.9–2.3
Hematite	0.0005–0.035	4.9–5.3

4 Results

4.1 Aeromagnetic data

4.1.1 Total magnetic intensity and reduction to the equator

The re-projected TMI grid, filtered to remove near-surface noise, has values from −43.9 to 198.0 nT (Fig. 6a). The RTE grid, computed with an inclination of −14.5° and a declination of −2.6°, ranges from −21.8 to 188.2 nT (Fig. 6b). The RTE map shows structure and lithological contrasts more clearly than the residual map. Four zones can be distinguished. Zone A is a high of 168.8–188.2 nT in the south-central part of the map. Zone B, with intermediate values of 119.9–163.3 nT, lies in the north-east and north-west around zone A. Zone C is a fairly low area of 65.7–107.8 nT in the south-east that extends towards the south-west, and zone D, the lowest, occupies the south-eastern edge and part of the north. The TMI and RTE maps differ slightly, mainly in the southern part.

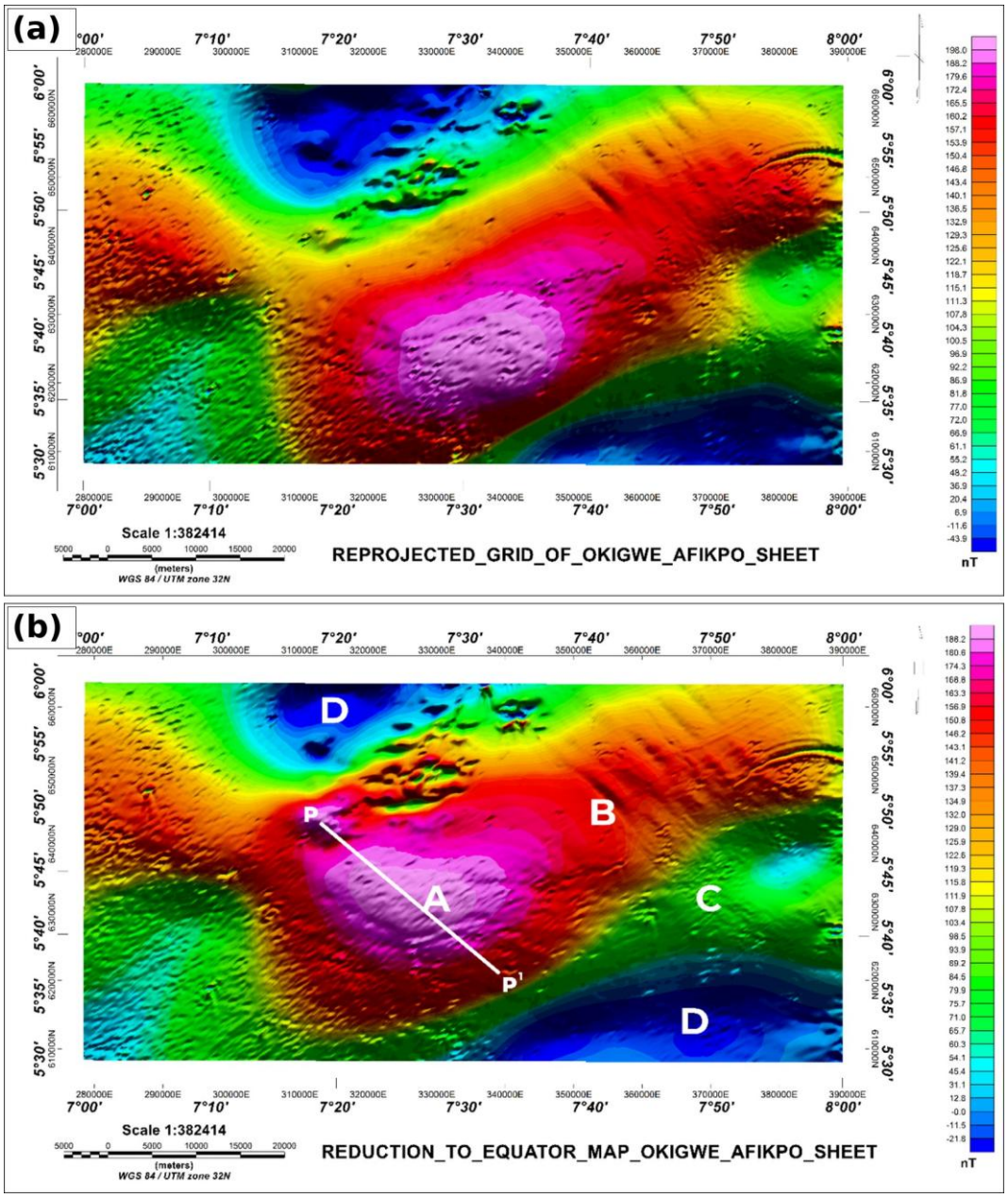

Fig. 6 (a) Re-projected total magnetic intensity (TMI) map and (b) TMI reduced to the equator (RTE)

4.1.2 Residual magnetic intensity

The residual map (Fig. 7) emphasises short-wavelength anomalies after removal of the regional field, and it reveals shallow anomalies that are masked in the RTE map (Fig. 6b) by deeper sources. It differs noticeably from the RTE map. Three areas, labelled H1, H2 and H3, are zones where basement rocks may be close to the surface. Their high values (18.6–30.7 nT) might reflect fresh basement rock. A minor linear feature with low magnetic values is visible in the northern part of the map, just below H2. The residual field ranges from −39.1 to 30.7 nT.

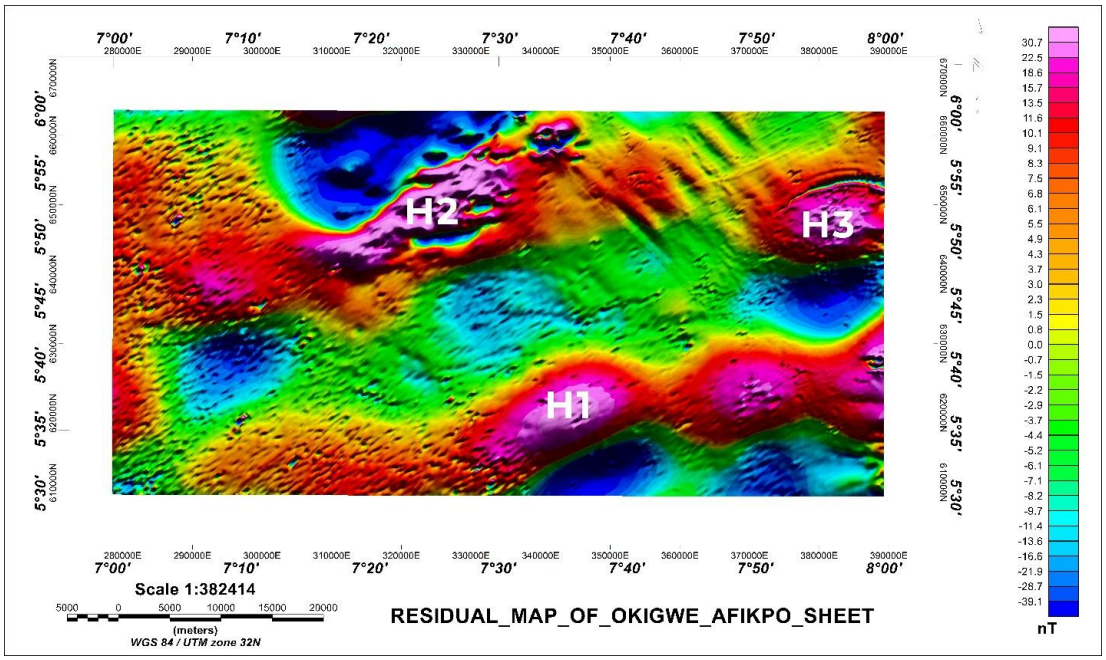

Fig. 7 Residual magnetic intensity map; H1–H3 mark possible near-surface basement highs

4.1.3 Upward continuation

Upward continuation of the RTE grid to 200 and 500 m (Fig. 8) suppresses shallow anomalies and gives a smoother, more regional view of the magnetic response of deeper sources (Roberts et al. 1990). Changes between the two levels are small at the regional edges. The field ranges from −19.2 to 186.2 nT at 200 m and from −15.7 to about 183 nT at 500 m. The continued maps show high positive anomalies extending from the north-east towards the north-west, and negative anomalies in the upper north and the south-east (Fig. 8b). Weakly magnetic, fractured rock is one possible explanation for the negative anomalies.

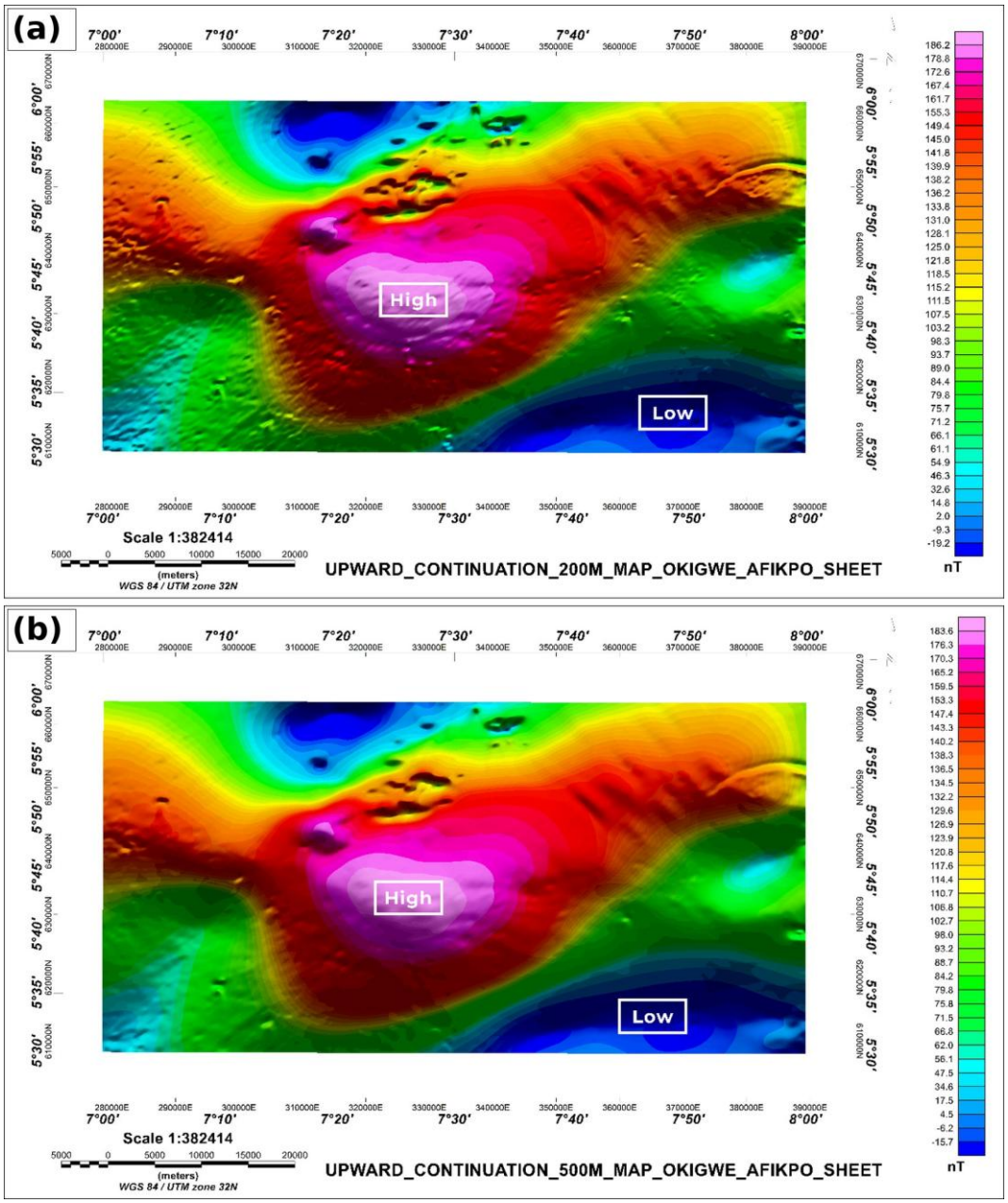

Fig. 8 Upward continuation of the RTE grid to (a) 200 m and (b) 500 m

4.1.4 Downward continuation

Downward continuation brings the observation surface closer to the sources and separates overlapping anomalies (Pawlowski 1995). The RTE grid was continued downward by 50 and 100 m (Fig. 9). The 50 m map ranges from −22.5 to 168.7 nT and the 100 m map from −23.3 to 189.3 nT. Both show features comparable to those of the RTE map (Fig. 6b).

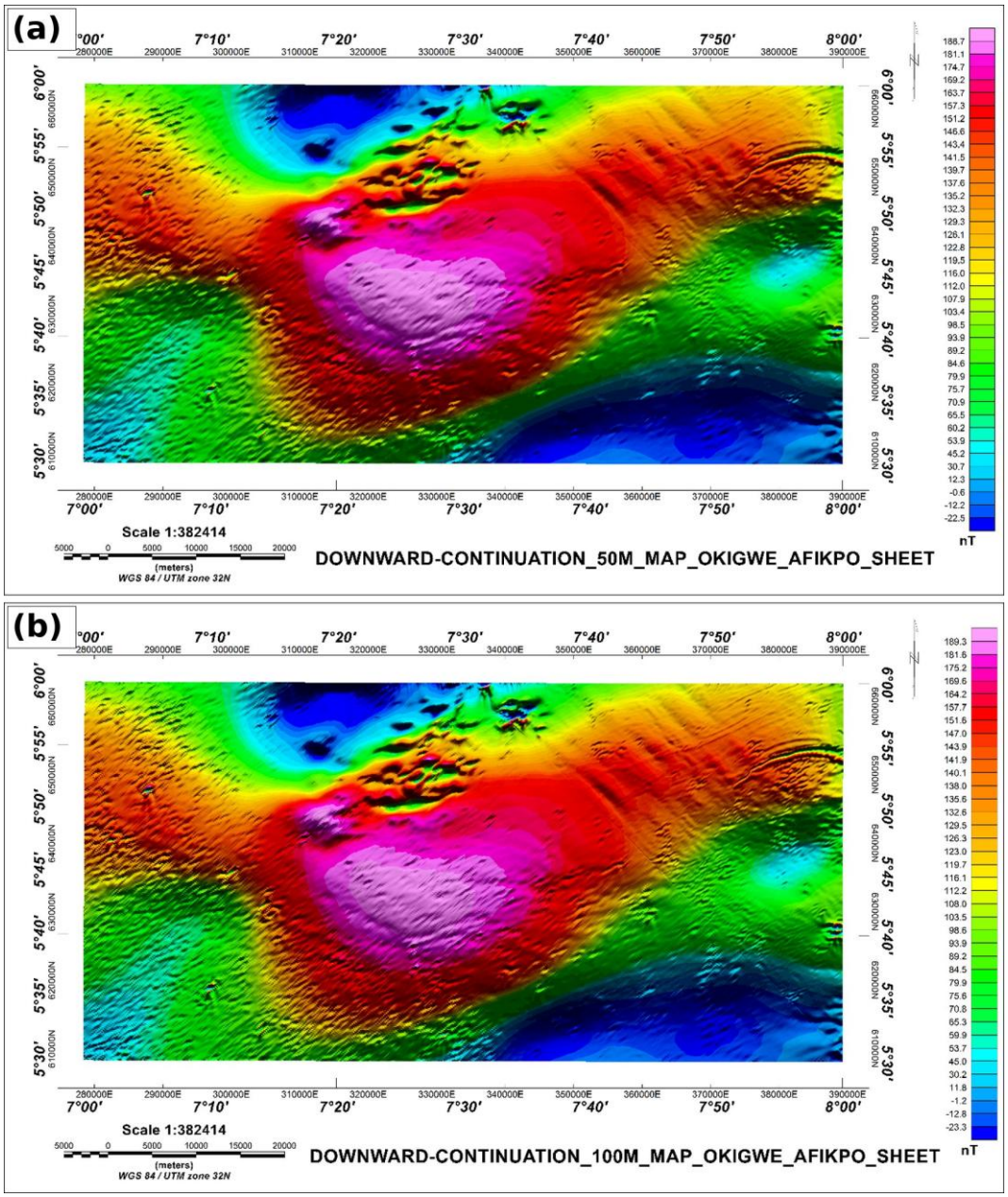

Fig. 9 Downward continuation of the RTE grid by (a) 50 m and (b) 100 m

4.1.5 Derivative maps

First-order derivatives peak where the field changes abruptly, so elongated maxima on the derivative maps indicate discontinuities and thus linear geological features (Fig. 10). These features trend NE–SW and ESE–WSW and are concentrated along lithological boundaries, which suggests intense deformation. The vertical derivative ranges from −0.02 to +0.01 nT m^{-1} (Fig. 10c), and the strongest responses may relate to ferromagnesian-rich rocks, which carry high magnetic susceptibility.

The THD (Fig. 11) images faults and contacts as narrow, straight ridges. It displays structures trending mainly NE–SW. The tilt derivative (Fig. 12) ranges from −1.34 to 1.41 rad and sharpens the curvature of near-vertical structures that arise from susceptibility contrasts, such as faults and shear or alteration zones.

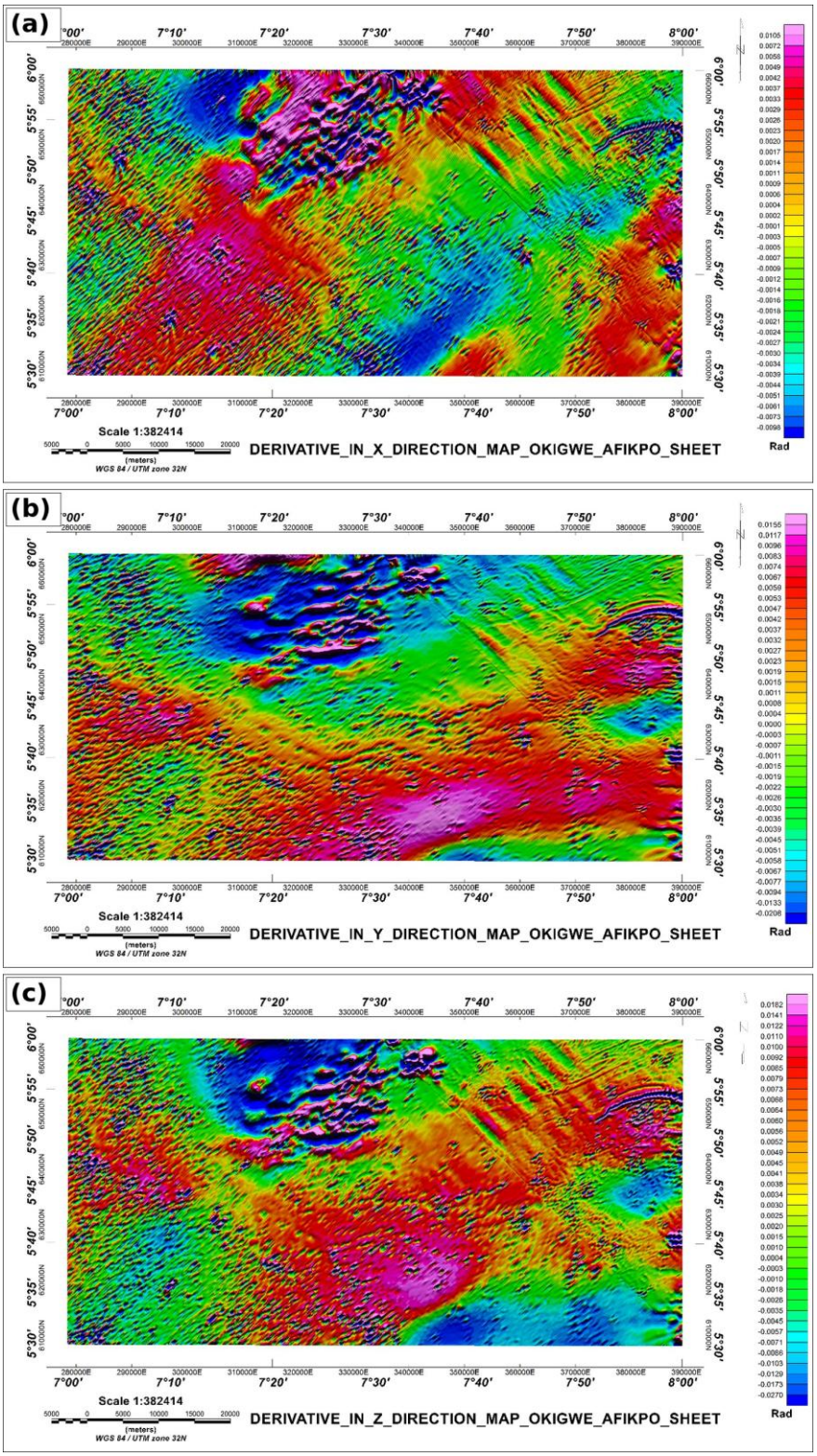

Fig. 10 First derivatives of the RTE grid in the (a) x, (b) y and (c) z directions

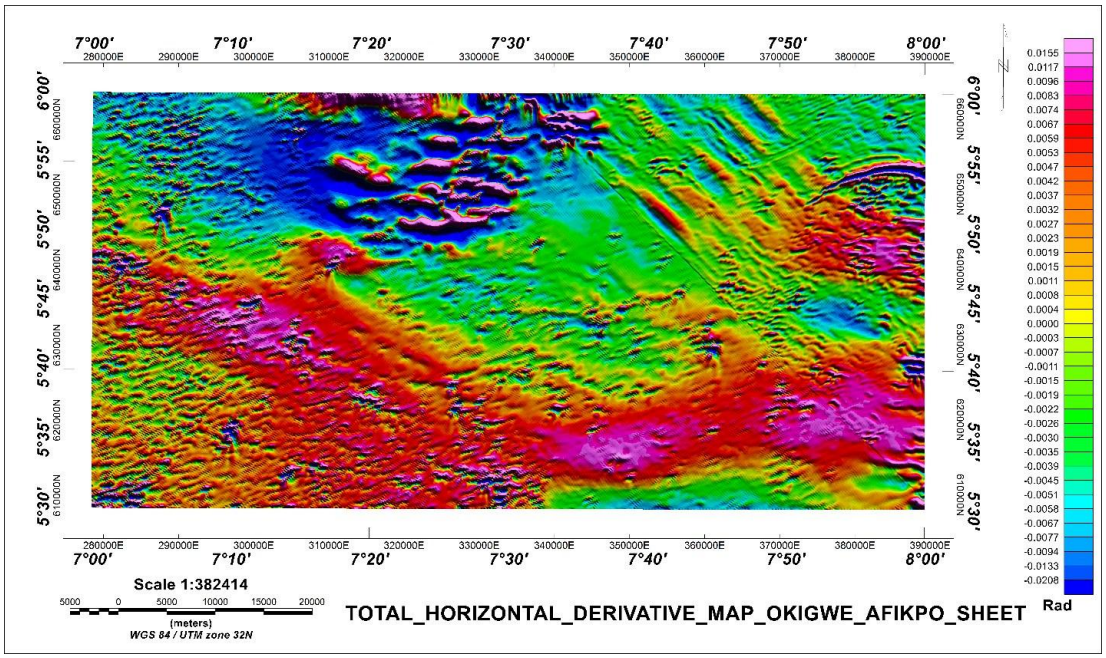

Fig. 11 Total horizontal derivative (THD) of the RTE grid

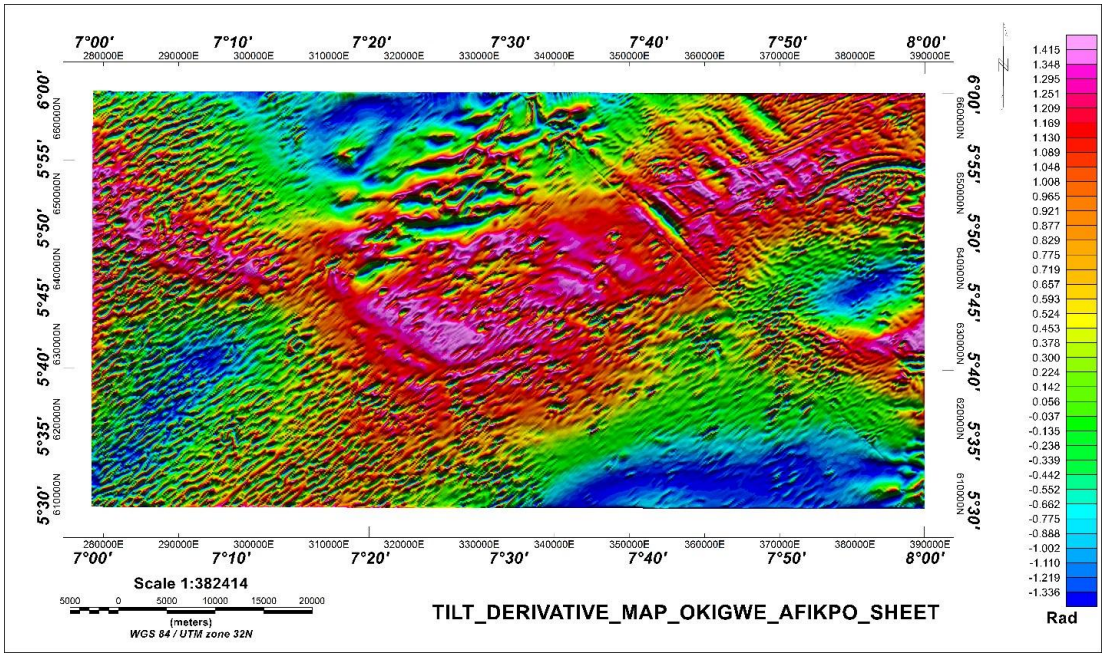

Fig. 12 Tilt derivative (TDR) of the RTE grid

4.1.6 Analytic signal and second vertical derivative

The analytic-signal amplitude (Fig. 13) ranges from 0.003 to 0.046 nT m^{-1}. High amplitudes (0.009–0.046 nT m^{-1}) occur mainly in the north and, more weakly, in the south, and they mark the edges of strongly magnetic or shallow sources. Prominent high-amplitude anomalies outline the limits of both positively and negatively magnetised sources. In this largely sedimentary terrain the strong responses are most plausibly produced by intrusive bodies, by ironstone-rich horizons or by uplifted basement blocks, although the data cannot distinguish between them.

The second vertical derivative map (Fig. 14) closely resembles the analytic-signal map. The northern high, labelled H, is clearer than on the analytic-signal map and indicates a shallow source with strong magnetisation.

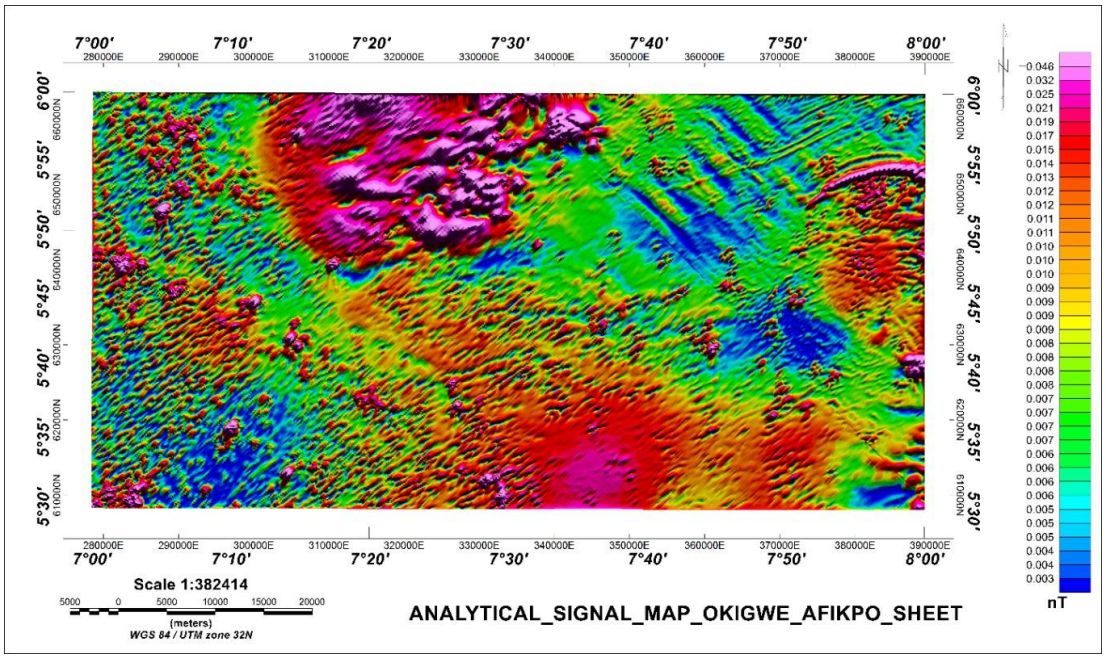

Fig. 13 Analytic-signal amplitude of the RTE grid

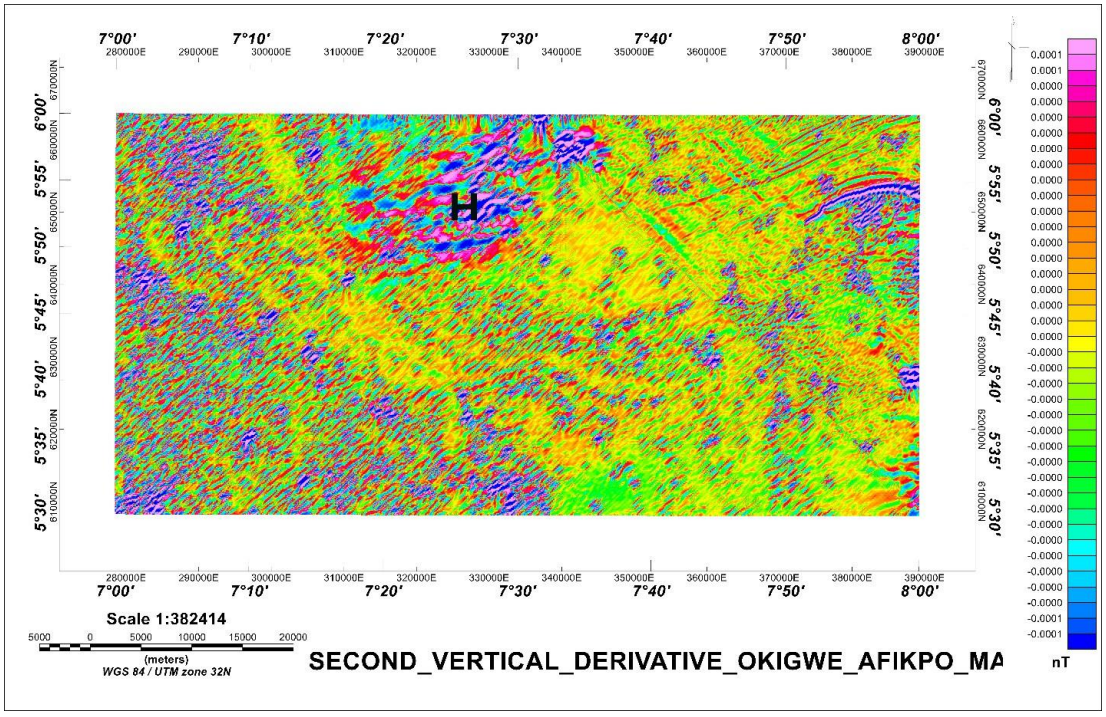

Fig. 14 Second vertical derivative (SVD) of the RTE grid; H marks a northern high

4.1.7 Lineaments

Lineaments extracted from the derivative maps (Fig. 15a) were summarised in a rose diagram (Fig. 15b). The dominant trend is NE–SW, with a subordinate E–W (ENE–WSW to ESE–WNW) set; the N–S trend is the least frequent. Most lineaments superimposed on the first vertical derivative map (Fig. 16) also

trend NE–SW. Lineaments in magnetic contours commonly follow regional geology, such as the strike of intrusive bodies or large faults (Dobrin and Savit 1988), and the NE–SW trend is parallel to the axis of the Benue Trough and to the fold trend of the Abakaliki Anticlinorium. Okoli et al. (2024) reported the same dominant NE–SW direction, with NW–SE and NNW–SSE to E–W sets, over a block that includes sheet 313, and Abdullahi and Kumar (2021) found NE–SW, ENE–WSW and WNW–ESE lineaments in the wider Anambra–Afikpo region. Because low magnetic latitude weakens the expression of E–W-striking sources, the E–W set might be under-represented.

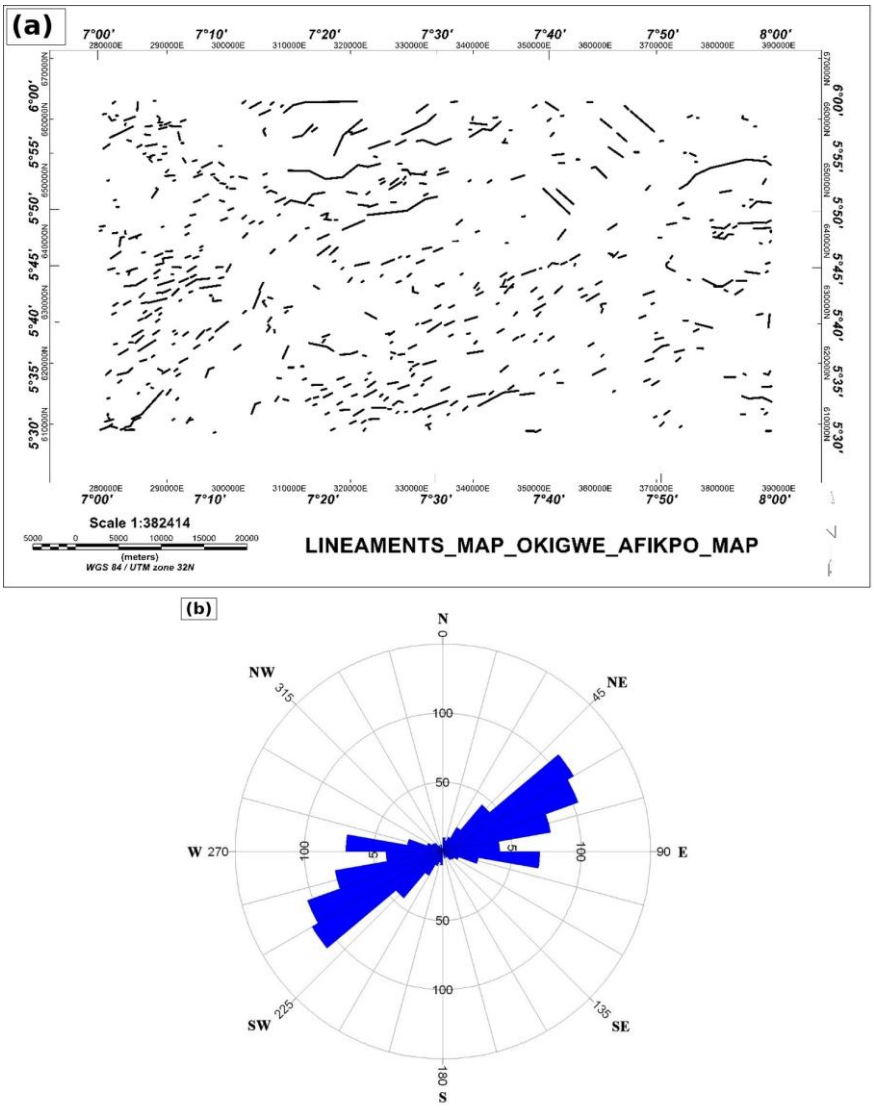

Fig. 15 (a) Lineaments interpreted from the RTE grid and (b) rose diagram of their trends

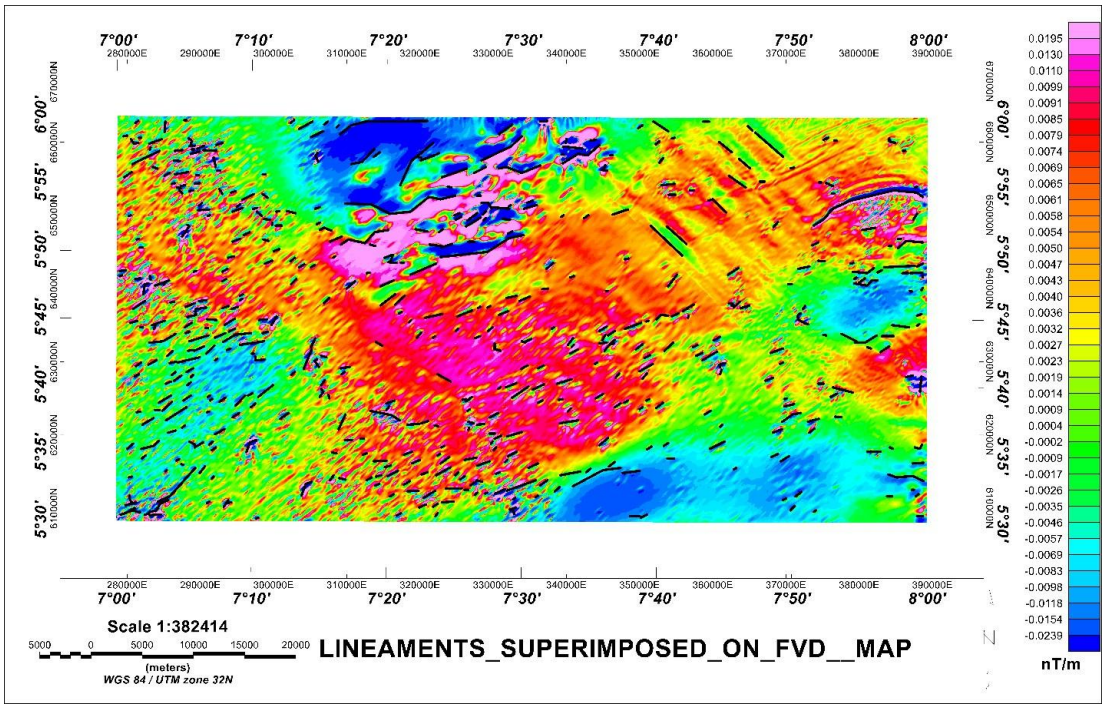

Fig. 16 Interpreted lineaments superimposed on the first vertical derivative map

4.1.8 Euler deconvolution

Euler deconvolution of the RTE grid with a structural index of 1.0 produced the solutions shown in Fig. 17. Source depths range from about 296 to 3,265 m. Solutions that align along a line at the same depth generally correspond to faults.

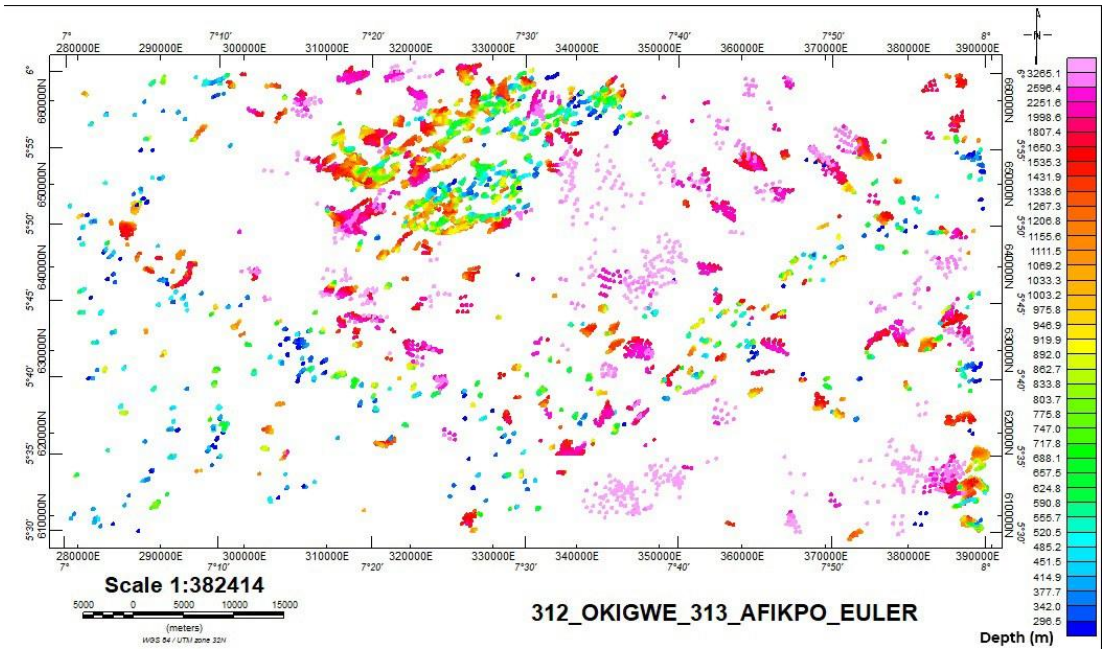

Fig. 17 Euler deconvolution solutions for the RTE grid (structural index 1.0)

4.1.9 Power spectrum

The radially averaged power spectrum of the magnetic anomaly (Fig. 18) was fitted with two linear segments, at about 0.02–0.17 and 0.28–0.48 in the wavenumber units of the figure. The deeper segment

gives depths to the top of the deeper source ensemble of 1.7–2.0 km, and the shallower segment gives depths above about 0.4 km. The deeper sources are associated with long-wavelength anomalies and possibly with basic intrusive rock at depth or dykes intruding at depth. The shallower ones correspond to short-wavelength anomalies.

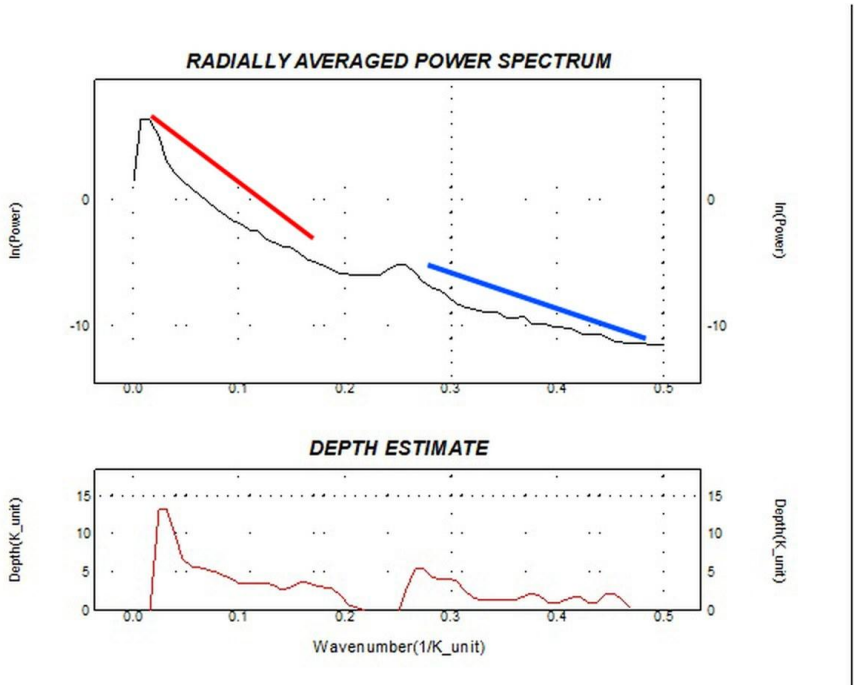

Fig. 18 Radially averaged power spectrum of the aeromagnetic anomaly, with fitted deep (red) and shallow (blue) segments and the associated depth estimates

4.1.10 Two-dimensional magnetic model

A two-dimensional model along profile P–P′ across the RTE map (Fig. 19) was built to estimate the depth to magnetic basement. The profile is about 34 km long. The model has a basement high at about 18 km along the profile, where the basement top lies at roughly 0.1–0.2 km, and the basement deepens to more than 1.5–2 km at the left end and towards the right end. The misfit reported by the software is 14.9 nT. The calculated curve does not reproduce the observed anomaly well (Section 5.5), so the model is preliminary.

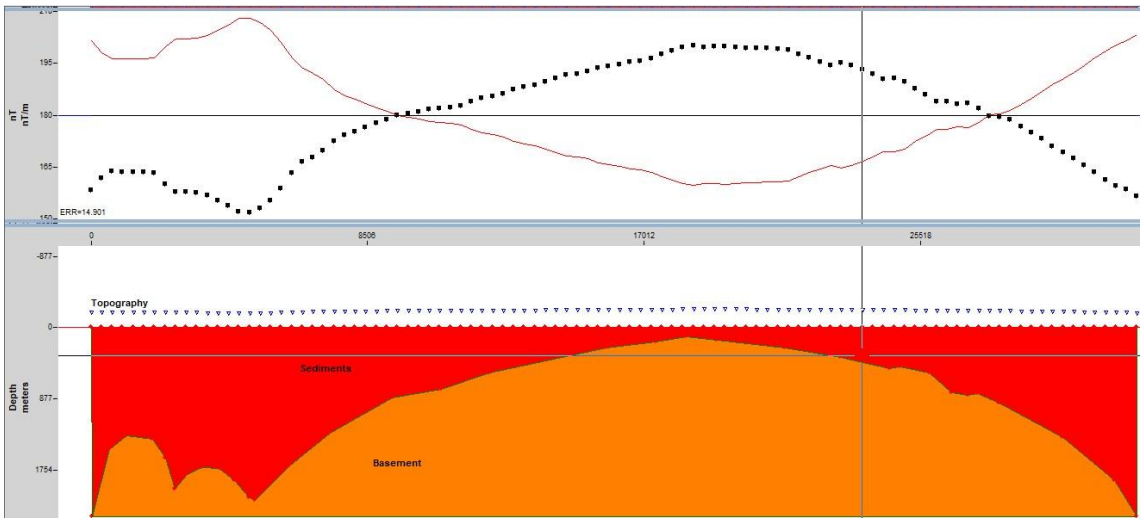

Fig. 19 Observed and calculated magnetic profiles and the two-dimensional subsurface model along profile P–P′ (RTE grid)

4.2 Gravity data

4.2.1 Bouguer anomaly

The Bouguer anomaly (Fig. 20) ranges from 7.8 to 57.6 mGal. A high of 48.9–57.6 mGal (feature A) lies in the north-central part of the area, and a low of 7.8–10.1 mGal (feature D) lies in the south. Features B and C have intermediate values and may mark fractured zones or the edges and contacts of different rock units. Faults inferred from the map trend mainly NE–SW. High values are generally taken to indicate denser rock, such as a shallow basement or intrusive body, and low values thicker sedimentary fill or less dense material.

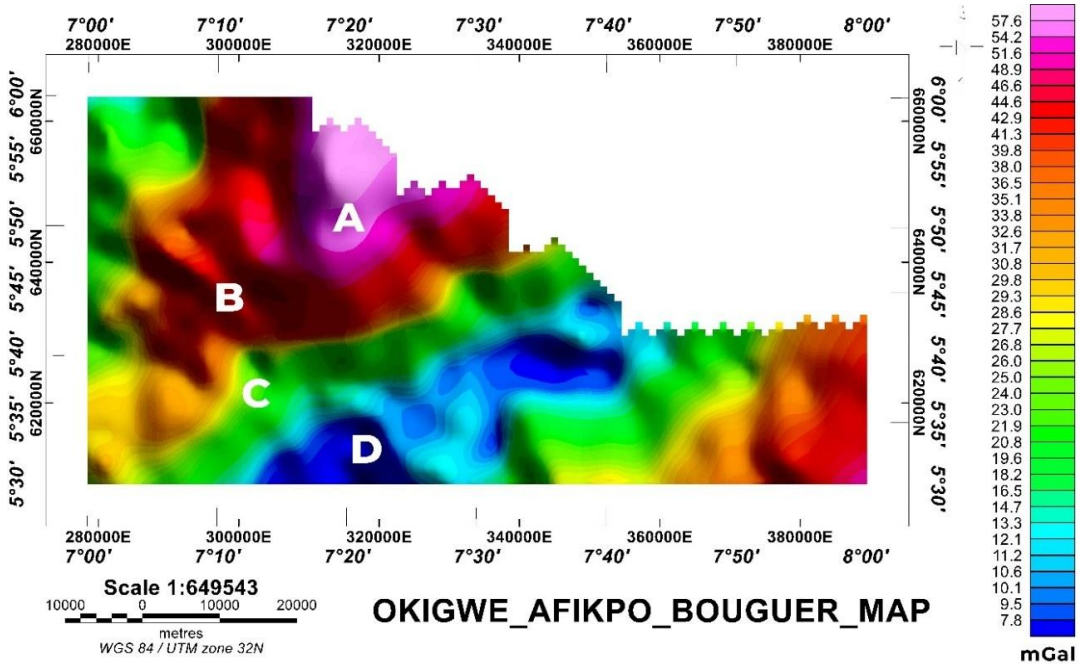

Fig. 20 Bouguer anomaly map of the Okigwe–Afikpo area; A–D mark the main features discussed in the text

4.2.2 Tilt derivative

The tilt-derivative map (Fig. 21) ranges from −1.41 to 1.39 rad. The region between the 0° and ±45° contours approximates the position of source margins and shallow basement (Al-Badani and Al-Wathaf 2017). Feature A coincides with an area of very high gravity values that probably reflects dense rock. Granitic bodies in the area may be linked to the north-western part of the map. In the south, weak zones bound the margins and trends of prominent lineaments, which run mainly towards the south-east.

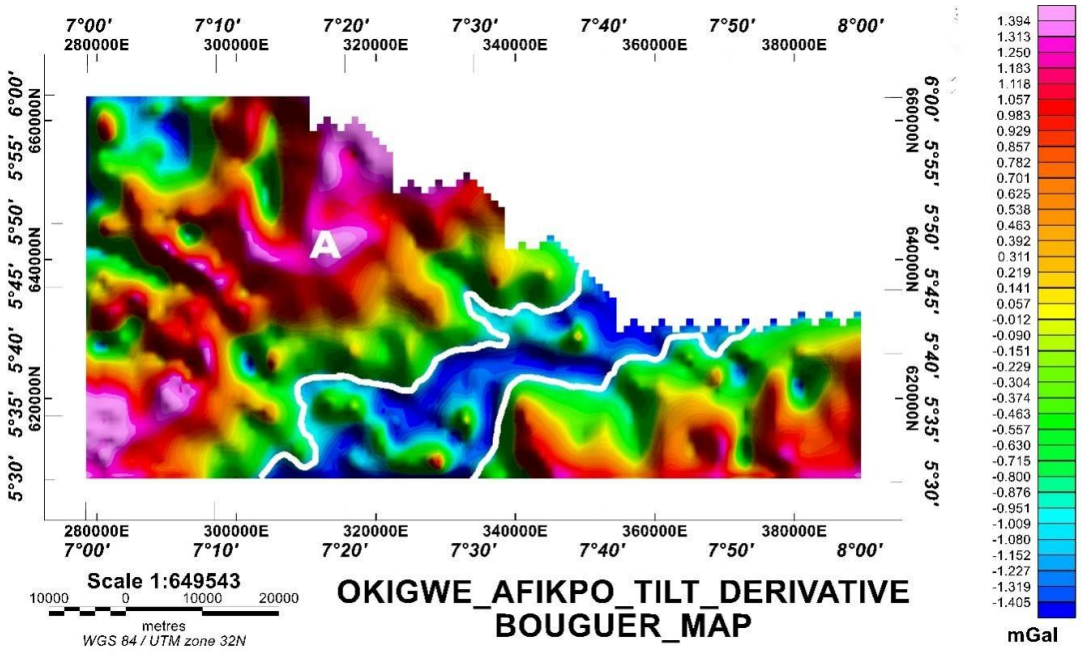

Fig. 21 Tilt derivative of the Bouguer anomaly

4.2.3 Downward continuation

Downward continuation of the Bouguer grid by 50 and 100 m (Fig. 22) produced ranges of 7.6–57.7 and 7.5–57.8 mGal and showed no significant change from the original map (Fig. 20). Anomaly separation therefore increases only at depths greater than 100 m, which suggests that the main density sources lie deeper than the continuation distances used.

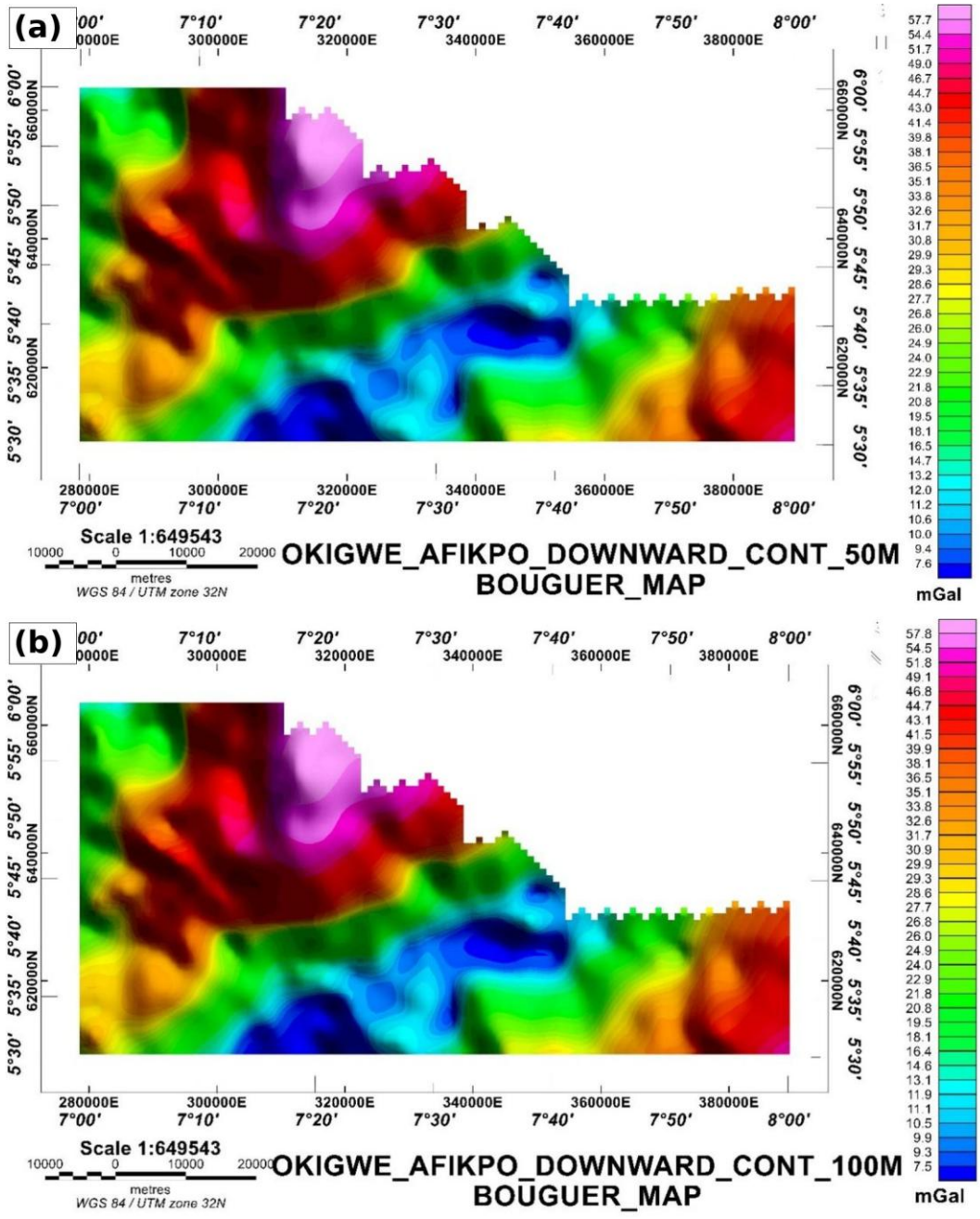

Fig. 22 Downward continuation of the Bouguer anomaly by (a) 50 m and (b) 100 m

4.2.4 Derivative maps

The first vertical derivative (Fig. 23a) sharpens anomalies above their sources, reduces anomaly complexity and gives clearer images of the causative bodies. Its main structural trend is NW–SE. The total horizontal derivative (Fig. 23b) shows effective structures trending N–S and NW–SE. The faults inferred from the Bouguer map itself trend NE–SW (Section 4.2.1), so the gravity gradients and the magnetic lineaments are not simply parallel.

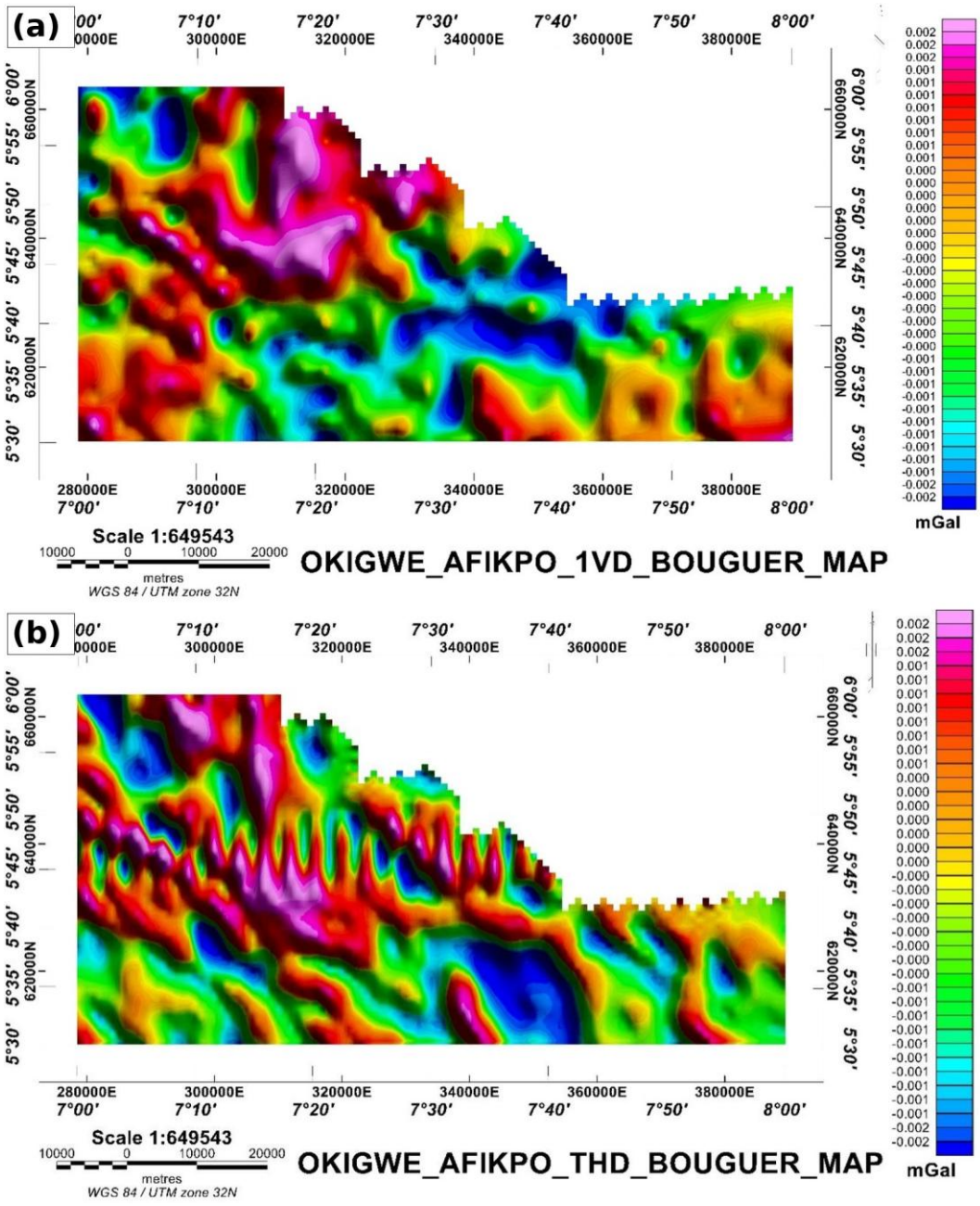

Fig. 23 (a) First vertical derivative and (b) total horizontal derivative of the Bouguer anomaly

4.2.5 Analytic signal

The analytic signal of the Bouguer anomaly (Fig. 24) exceeds 0.003 mGal m^{-1} in places scattered along a NW–SE band, whereas the lowest amplitudes (about 0.001 mGal m^{-1}) occur in the south-east and along the north-west. The high values can be attributed to dense, shallow rock bodies, and the low values to less dense, highly broken rock. As the study area is mainly a sedimentary terrain, granitic or gneissic basement is more likely to be present at depth, as part of the crystalline basement or as uplifted blocks, than at the surface.

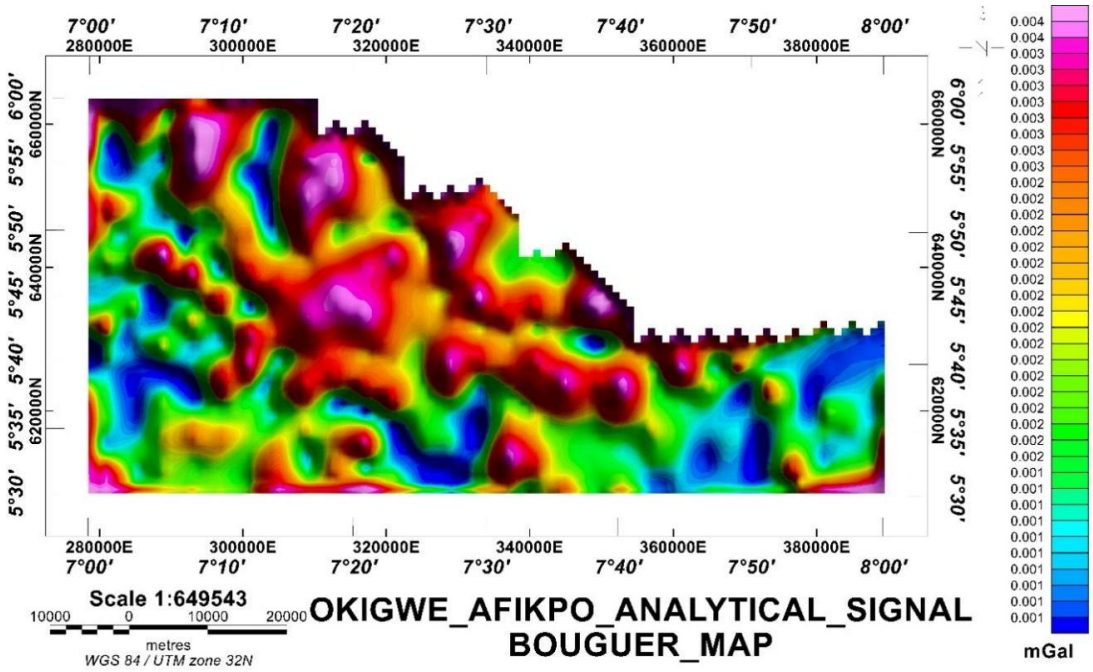

Fig. 24 Analytic signal of the Bouguer anomaly

4.2.6 Euler deconvolution

Euler deconvolution of the Bouguer grid (Fig. 25) was run for a single structural index. The best solutions cluster in a few parts of the area rather than spreading evenly, and they extend to depths of more than 2,000 m.

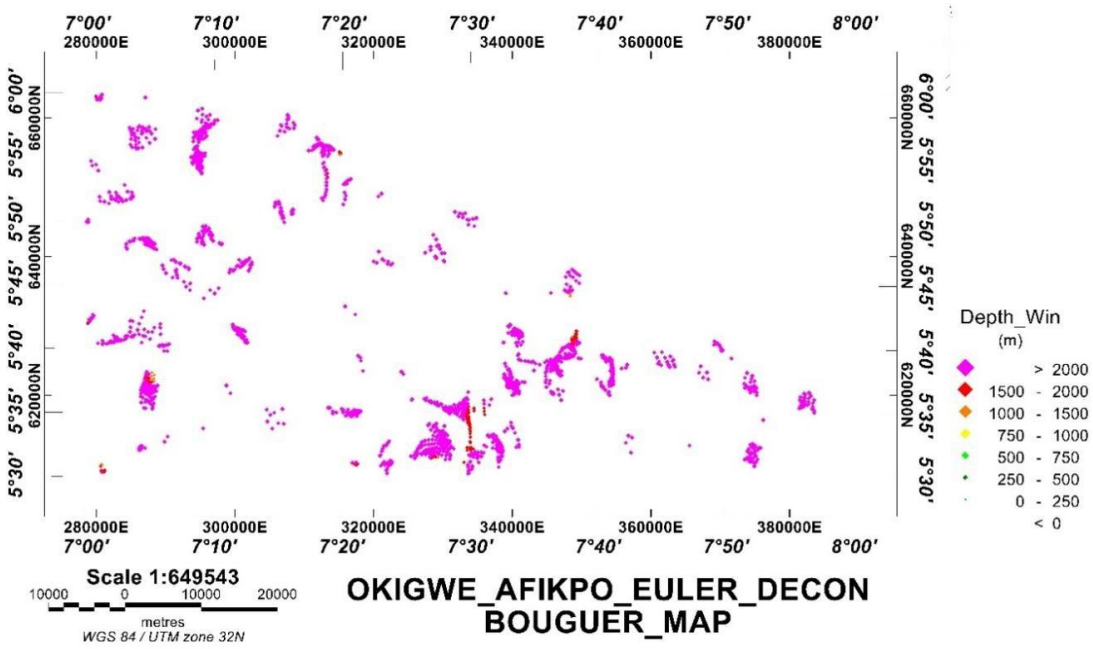

Fig. 25 Euler deconvolution solutions for the Bouguer anomaly

4.2.7 Two-dimensional gravity model

A two-dimensional model along one gravity profile (Fig. 26) was built with GM-SYS to assess the depth to the top of the basement. The profile is about 47 km long and comprises a sediment layer above a

basement layer. The basement top lies at roughly 0.1–0.2 km at about 23 km along the profile, rises to about 0.7 km near 6 km, falls to about 1.25 km near 12 km and reaches 1.7–1.9 km at the eastern end. The misfit reported by the software is 10.5 mGal. As with the magnetic model, the calculated curve departs substantially from the observed one (Section 5.5). Table 2 lists the ranges of all the processed magnetic and gravity maps.

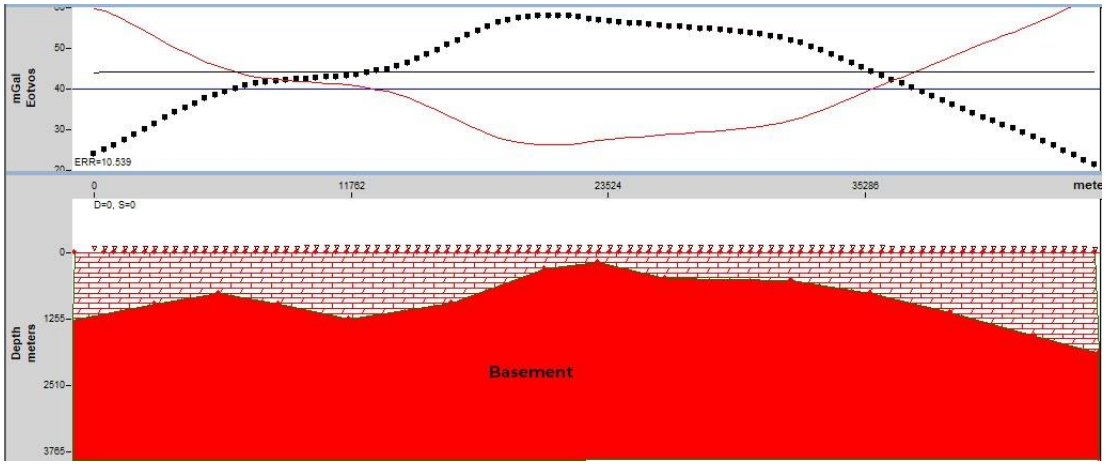

Fig. 26 Observed and calculated gravity profiles and the two-dimensional basement model along the gravity profile

Table 2 Ranges of the magnetic and gravity maps (values as measured on the processed grids)

Map	Range	Unit
Magnetic data		
Total magnetic intensity (TMI)	−43.9 to 198.0	nT
Reduced to the equator (RTE)	−21.8 to 188.2	nT
Residual field	−39.1 to 30.7	nT
Upward continuation, 200 m	−19.2 to 186.2	nT
Upward continuation, 500 m	−15.7 to ≈183	nT
Downward continuation, 50 m	−22.5 to 168.7	nT
Downward continuation, 100 m	−23.3 to 189.3	nT
Analytic signal	0.003 to 0.046	nT m^{-1}
Tilt derivative	−1.34 to 1.41	rad
Euler depth (SI = 1.0)	296 to 3,265	m
Gravity data		
Bouguer anomaly	7.8 to 57.6	mGal
Downward continuation, 50 m	7.6 to 57.7	mGal
Downward continuation, 100 m	7.5 to 57.8	mGal
Analytic signal	0.001 to 0.004	mGal m^{-1}
Tilt derivative	−1.41 to 1.39	rad
Euler depth	> 2,000	m

5 Discussion

5.1 Depth estimates and comparison with earlier work

The depth estimates in this study (Table 2) fall into three groups; Table 3 compares them with earlier estimates. Euler solutions for the magnetic field lie between about 0.3 and 3.3 km, the spectral analysis gives shallow sources above 0.4 km and deeper sources at 1.7–2.0 km, and the preliminary profile models place the top of the basement between about 0.1 km over the highs and about 2 km towards the profile ends. Euler solutions for the gravity field extend to more than 2 km. The magnetic and gravity depth ranges therefore overlap, and both point to a basin floor whose depth varies laterally rather than a uniformly deep trough. The depths quoted by different methods are not equivalent, however. Spectral depths describe the top of a source ensemble, Euler depths describe individual sources, and the models describe an interface, so that overlap between the ranges is not by itself proof that the methods agree.

Table 3 Depth estimates from this and earlier studies in and near the study area

Study	Area	Method	Reported depth
This study	Okigwe–Afikpo (sheets 312, 313)	Euler, RAPS, 2-D models (magnetic and gravity)	0.3–3.3 km (Euler); 1.7–2.0 and < 0.4 km (RAPS); 0.1 to > 2 km (2-D models)
Ofoegbu and Onuoha (1991)	Abakaliki Anticlinorium	2-D spectral analysis, aeromagnetic	Deeper sources 1.2–2.5 km
Ugwu et al. (2013)	Okigwe and Afikpo sheets	Forward and inverse modelling, aeromagnetic	3.0–12.7 km (buried anomalous bodies)
Oha et al. (2016)	Southern Benue Trough	3-D Euler, SPI, aeromagnetic	Maxima 4.40 and 4.85 km; means 0.42 and 0.37 km
Onuba et al. (2013)	Afikpo–Ogoja axis	Spectral analysis, aeromagnetic	Shallow 0.1–1.68 km; deeper 1.87–3.98 km
Abdullahi and Kumar (2021)	Anambra Basin, Abakaliki Anticlinorium, Afikpo Syncline	Three magnetic methods and a 2-D gravity model	8.4–9.1, 3.1–9.8 and 3.8–8.5 km respectively
Ijeh et al. (2025)	Okigwe (sheet 312)	Spectral analysis and SPI, aeromagnetic	Deeper 1.86–3.79 km (mean 2.53 km); shallower 0.22–0.48 km (mean 0.34 km)

RAPS, radially averaged power spectrum; SPI, source parameter imaging. The depths are quoted as reported and refer to different physical quantities.

Our shallow and deeper spectral depths and the range of the Euler solutions are of the same order as the spectral results that Ijeh et al. (2025) obtained for the Okigwe sheet (Table 3). They also fit the 1.2–2.5 km deeper sources found by Ofoegbu and Onuoha (1991) over the Abakaliki Anticlinorium and the mean depth of 0.42 km that Oha et al. (2016) reported for shallow intrusions in the southern Benue Trough. They are shallower than the 3.8–8.5 km that Abdullahi and Kumar (2021) obtained for the Afikpo Basin, whose estimates combine several methods with a gravity model and apply to a wider area, and than the 3.0–12.7 km that Ugwu et al. (2013) assigned to modelled intrusive bodies. The latter range refers to bodies emplaced in sediments or basement and not to the basement surface, so it does not constrain sediment thickness directly. The largest depths in our results (about 3.3 km) are comparable

to the 3 km thickness that Osinowo and Taiwo (2020) used to identify parts of the Lower Benue Trough worth further petroleum investigation.

5.2 Structural framework

The dominant NE–SW lineament trend parallels the axis of the Benue Trough and the fold trend of the Abakaliki Anticlinorium, which are attributed to reactivated basement fabric and to Santonian compression (Benkhelil 1989; Odigi and Amajor 2009). The same trend dominates over a block that includes sheet 313 (Okoli et al. 2024) and in the wider Anambra–Afikpo region (Abdullahi and Kumar 2021). The E–W to ENE–WSW set may reflect transverse structures or older basement fabric. Because E–W-striking sources are weakly expressed at low magnetic latitude, the E–W set should be treated with caution. The gravity gradients show NW–SE and N–S trends and the Bouguer map shows NE–SW faults, a combination that suggests a block-faulted basement in which gravity gradients and magnetic lineaments partly coincide and partly cross. Quantitative statistics on trend intervals and lengths would be needed to test this.

The study area is part of a segmented basin floor. Basement highs of limited extent, such as zones A and H1–H3 on the magnetic maps and feature A on the gravity map, alternate with deeper areas such as gravity low D and the south-eastern magnetic lows. This arrangement resembles the fragmented, block-faulted basement floor described for the southern Benue Trough by Adebiyi et al. (2023).

5.3 Relationship between the magnetic and gravity fields

The two fields correspond in some places and disagree in others. In the north, the strong analytic-signal and SVD responses (feature H) and the north-central gravity high (feature A) occur in the same part of the map, which suggests a dense, magnetic source close to the surface, such as a basement high or intrusive body. In the south, the opposite pattern appears: the south-central magnetic high (zone A) lies over or near the gravity low (feature D). That combination is compatible with thick, low-density sediment that contains magnetic intrusive bodies or ironstone-rich horizons, but it could also reflect a deeper magnetic basement beneath a thick non-magnetic cover. In the south-east, magnetic lows (zones C and D) coincide with intermediate gravity values. A low magnetic anomaly over a gravity high can result from dense but weakly magnetic rock, from non-magnetic sediments over dense basement, from the negative central response of a susceptible body at low magnetic latitude, from remanent magnetisation, or from interference between sources. Because an induced anomaly at the equator is negative over the centre of a compact body, the polarity of the RTE anomaly alone cannot be used to assign susceptibility or lithology. The analytic signal and THD, which do not depend on sign, are better guides to the position of sources. Resolving the discordant zones would require a quantitative joint treatment, such as a pseudo-gravity transform of the magnetic field with correlation analysis, which was not carried out here.

5.4 Implications for mineral and hydrocarbon investigation

Potential-field data constrain structure and approximate depth. They cannot establish source-rock richness, kerogen type, thermal maturity, migration timing, or the presence of reservoir, seal and trap. A sedimentary thickness of about 2–3 km is therefore permissive rather than diagnostic: it shows that enough sediment exists to be of interest but not that hydrocarbons were generated. Two cautions apply. First, shallow intrusions cut the succession in the southern Benue Trough (Oha et al. 2016; Adebiyi et al. 2020), and they may raise thermal maturity locally or compartmentalise reservoirs. Second, the Nkporo Group and the Imo and Nsukka formations are only locally expected to reach the maturity needed for expulsion in the Anambra Basin (Reijers and Nwajide 1998). The Okigwe part of the Anambra Basin, where the sedimentary cover reaches about 2–3 km in our estimates, could therefore be considered for seismic and geochemical evaluation. The zones of thicker fill identified here are candidates for such work, but that is a statement about where to look, not about prospectivity.

The NE–SW lineaments and the shallow, strongly magnetic bodies are also targets for mineral exploration. Faults can act as conduits for mineralising fluids, and Pb–Zn(–Cu) mineralisation is documented elsewhere in the Lower Benue Trough (Olade and Morton 1985; Akande and Mücke 1993). Whether the structures mapped here relate to such mineralisation cannot be decided from these data. They should be compared with known occurrences and tested by geochemical sampling and, where justified, core drilling. Fracture zones are also commonly targeted for groundwater in low-permeability terrain, so the lineament map may serve as a screening layer for borehole siting once it has been validated by electrical resistivity surveys.

5.5 Limitations

Several limitations affect the results. First, potential-field depth estimates are non-unique and are not calibrated against boreholes or seismic data. Second, the two profile models fit the observed data poorly. In both cases the calculated curve departs substantially from the observed one (misfits of 14.9 nT and 10.5 mGal for the magnetic and gravity profiles respectively), and the models do not constrain densities or susceptibilities. They illustrate one possible basement geometry and should not be read as a final basin model. Third, a single profile cannot establish the number or extent of sub-basins. Fourth, the Euler solutions depend on the structural index and window size, and a single index was used for each field. Fifth, the low magnetic latitude weakens the expression of E–W-striking sources and biases directional derivatives. Finally, the gravity data are described only in general terms in this study, and the reduction density and terrain correction should be documented before interpretations that depend on absolute density are made.

6 Conclusions

The aeromagnetic and gravity data of the Okigwe–Afikpo area (sheets 312 and 313) reveal a segmented basement and a basin floor of variable depth. The main conclusions are as follows.

1. The RTE magnetic anomaly ranges from −21.8 to 188.2 nT and the Bouguer anomaly from 7.8 to 57.6 mGal. The main magnetic features are a high in the south-central area, intermediate values around it, and lows in the south-east and north. The main gravity features are a high in the north-central area and a low in the south.

2. Magnetic lineaments trend mainly NE–SW, parallel to the Benue Trough and the Abakaliki fold belt, with a subordinate E–W set. Gravity gradients trend mainly NW–SE and N–S. The lineaments are interpreted as possible faults, contacts or dyke-like bodies.

3. Magnetic Euler solutions lie between about 296 and 3,265 m, spectral analysis gives deeper sources at 1.7–2.0 km and shallower sources above 0.4 km, and gravity Euler solutions reach more than 2,000 m. These depths agree with several earlier spectral estimates and are shallower than those from combined magnetic–gravity studies of a wider area.

4. Two preliminary profile models place the basement top at about 0.1–0.2 km beneath central highs and at more than 1.2–2 km towards the ends of the profiles. Both models need refinement before they can be used quantitatively.

5. The zones of thicker sediment, the basement highs and the NE–SW structural corridors are targets for seismic, geochemical, drilling and hydrogeological follow-up. Potential-field data alone do not demonstrate hydrocarbon or mineral prospects.

Further work should include re-modelling of the profiles with constrained densities and susceptibilities, three-dimensional inversion of both fields, quantitative joint analysis of the magnetic and gravity data, aeroradiometric interpretation, ground follow-up and geochemical surveys, and the calibration of depths against boreholes and seismic data.

Declarations

Funding

No external funding statement was available in the source material reviewed for this manuscript.

Ethical Approval

This study involves airborne magnetometry and solid mineral exploration data analysis without human or animal subjects. Ethical approval was not required for this research.

Consent to Participate

Not applicable. This study did not involve human participants or personal data collection.

Consent to Publish

Not applicable. This study does not contain any individual person's data in any form (including individual details, images, or videos).

Data Availability: The Aeromagnetic dataset from Nigerian Geological Survey Agency (NGSA) and interpretations are available from the corresponding author.

Ethics Statement: The dataset was acquired by Nigerian Geological Survey Agency (NGSA) and was released for academic research. no human or animal subjects were involved.

References

Abdullahi M, Kumar R (2021) Basement and structure near the southwestern margin of the lower Benue Trough between, and including, the Anambra Basin and Afikpo Syncline, as derived from aeromagnetic and gravity data. Pure Appl Geophys 178:3953–3970. https://doi.org/10.1007/s00024-021-02801-3

Abdullahi M, Kumar R, Idi BY, Singh UK, Abba AU (2023) Analysis of recent airborne gravity and magnetic data for the interpretation of basement structures underneath the south-western Benue Trough using source edge detector filters. Acta Geophys 71:1595–1606. https://doi.org/10.1007/s11600-023-01060-1

Abdullahi M, Singh UK, Roshan R (2019) Mapping magnetic lineaments and subsurface basement beneath parts of Lower Benue Trough (LBT), Nigeria: insights from integrating gravity, magnetic and geologic data. J Earth Syst Sci 128:17

Adebiyi LS, Eluwole AB, Fajana AO, Salawu NB, Saleh A (2023) Contrasting structures of the Southern Benue trough and the contiguous crystalline basement as observed from high-resolution aeromagnetic data. Sci Rep 13:21516. https://doi.org/10.1038/s41598-023-48639-8

Adebiyi LS, Fatoba JO, Salawu NB, Dopamu KO, Abdulraheem TY, Obaseki OS, Olasunkanmi NK, Adediran SO (2020) Analysis of aeromagnetic data: application to Early–Late Cretaceous events in parts of Lower Benue trough, Southern Nigeria. J Appl Geophys 178:104052

Akande SO, Mücke A (1993) Co-existing copper sulphides and sulphosalts in the Abakaliki Pb–Zn deposit, Lower Benue Trough and their genetic implications. Mineral Petrol 47:183–192. https://doi.org/10.1007/BF01161566

Al-Badani MA, Al-Wathaf YM (2017) Using the aeromagnetic data for mapping the basement depth and contact locations, at southern part of Tihamah region, western Yemen. Egypt J Pet 27:485–495

Alken P, Thébault E, Beggan CD et al (2021) International Geomagnetic Reference Field: the thirteenth generation. Earth Planets Space 73:49

Baranov V (1957) A new method for interpretation of aeromagnetic maps: pseudo-gravimetric anomalies. Geophysics 22:359–383

Barbosa VCF, Silva JBC, Medeiros WE (1999) Stability analysis and improvement of structural index estimation in Euler deconvolution. Geophysics 64:48–60

Benkhelil J (1989) The origin and evolution of the Cretaceous Benue Trough (Nigeria). J Afr Earth Sci 8:251–282. https://doi.org/10.1016/S0899-5362(89)80028-4

Benkhelil J, Robineau B (1983) Is the Benue Trough a rift? Bull Cent Rech Explor-Prod Elf-Aquitaine 7:315–321

Burke KC, Dessauvagie TFJ, Whiteman AJ (1972) Geological history of the Benue Valley and adjacent areas. In: Dessauvagie TFJ, Whiteman AJ (eds) African geology. Ibadan University Press, Ibadan, pp 187–205

Chiaghanam OI, Ikegwuonu ON, Chiadikobi KC, Omoboriowo AO (2012) Sequence stratigraphy and palynological analysis of late Campanian to Maastrichtian sediments in the Upper Cretaceous, Anambra Basin: a case study of Okigwe and its environs, south-eastern Nigeria. Adv Appl Sci Res 3:964

Cooley JW, Tukey JW (1965) An algorithm for the machine calculation of complex Fourier series. Math Comput 19:297–301

Dean WC (1958) Frequency analysis for gravity and magnetic interpretation. Geophysics 23:97–127

Dobrin MB, Savit CH (1988) Introduction to geophysical prospecting, 4th edn. McGraw-Hill, New York

FitzGerald D, Reid A, McInerney P (2004) New discrimination techniques for Euler deconvolution. Comput Geosci 30:461–469

Grant NK (1971) The South Atlantic, Benue Trough, and Gulf of Guinea Cretaceous triple junction. Geol Soc Am Bull 82:2295–2298

Henderson RG, Zietz I (1949) The upward continuation of anomalies in total magnetic intensity fields. Geophysics 14:517–534

Hinze WJ, von Frese RRB, Saad AH (2013) Gravity and magnetic exploration: principles, practices, and applications. Cambridge University Press, Cambridge

Hoque M, Nwajide CS (1984) Tectono-sedimentological evolution of an elongate intracratonic basin (aulacogen): the case of the Benue Trough of Nigeria. J Min Geol 21:19–26

Hunt CP, Moskowitz BM, Banerjee SK (1995) Magnetic properties of rocks and minerals. In: Ahrens TJ (ed) Rock physics and phase relations: a handbook of physical constants. American Geophysical Union, Washington DC, pp 189–204

Igwesi DI, Umego MN (2013) Interpretation of aeromagnetic anomalies over some parts of the Lower Benue Trough using spectral analysis technique. Int J Sci Technol Res 2:132–138

Ijeh BI, Ahamefule CY, Azunna DE, Onyebere BC, Anyadiegwu FC (2025) Evaluation of the geothermal potential of Okigwe and environs using aeromagnetic method. UNIZIK J Eng Appl Sci 5:2552–2567

Kearey P, Brooks M, Hill I (2002) An introduction to geophysical exploration, 3rd edn. Blackwell, Oxford

MacLeod IN, Vieira S, Chaves AC (1993) Analytic signal and reduction-to-the-pole in the interpretation of total magnetic field data at low magnetic latitudes. In: Proceedings of the 3rd International Congress of the Brazilian Geophysical Society, pp 831–835

Miller HG, Singh V (1994) Potential field tilt—a new concept for location of potential field sources. J Appl Geophys 32:213–217

Murat RC (1972) Stratigraphy and paleogeography of the Cretaceous and Lower Tertiary in southern Nigeria. In: Dessauvagie TFJ, Whiteman AJ (eds) African geology. Ibadan University Press, Ibadan, pp 251–266

Nabighian MN (1972) The analytic signal of two-dimensional magnetic bodies with polygonal cross-section: its properties and use for automated anomaly interpretation. Geophysics 37:507–517. https://doi.org/10.1190/1.1440276

NEITI (2024) 2022/2023 Solid minerals industry report. Nigeria Extractive Industries Transparency Initiative, Abuja

Nwachukwu SO (1972) The tectonic evolution of the southern portion of the Benue Trough, Nigeria. Geol Mag 109:411–419

Nwajide CS (2005) Anambra Basin of Nigeria: synoptic basin analysis as a basis for evaluating its hydrocarbon prospectivity. In: Okogbue CO (ed) Hydrocarbon potentials of the Anambra Basin: geology, geochemistry and geohistory perspectives. Great AP Express, Nsukka, pp 1–46

Nwajide CS (2013) Geology of Nigeria's sedimentary basins. CSS Bookshops, Lagos

Odigi MI, Amajor LC (2009) Brittle deformation of the Afikpo Basin, SE Nigeria: evidence for a terminal Cretaceous extensional regime in the Lower Benue Trough. Chin J Geochem 28:369–376. https://doi.org/10.1007/s11631-009-0369-2

Ofoegbu CO (1985) A review of the geology of the Benue Trough, Nigeria. J Afr Earth Sci 3:283–291

Ofoegbu CO, Onuoha KM (1991) Analysis of magnetic data over the Abakaliki Anticlinorium of the Lower Benue Trough, Nigeria. Mar Pet Geol 8:174–183. https://doi.org/10.1016/0264-8172(91)90005-L

Oha IA, Onuoha KM, Nwegbu AN, Abba AU (2016) Interpretation of high resolution aeromagnetic data over southern Benue Trough, southeastern Nigeria. J Earth Syst Sci 125:369–385. https://doi.org/10.1007/s12040-016-0666-1

Okoli EO, Obiadi II, Obiadi CM, Ezim OE, Okeke GC, Irumhe EP, Mgbolu CC, Odiegwu JC (2024) Lithological and structural characterization of parts of the Lower Benue Trough, Southeast Nigeria, using radiometric and aeromagnetic data. Asian J Earth Sci 17:1–14. https://doi.org/10.3923/ajes.2024.01.14

Olade MA (1975) Evolution of Nigeria's Benue Trough (aulacogen): a tectonic model. Geol Mag 112:575–583

Olade MA, Morton RD (1985) Origin of lead-zinc mineralization in the southern Benue Trough, Nigeria: fluid inclusion and trace element studies. Miner Deposita 20:76–80. https://doi.org/10.1007/BF00204313

Onuba LN, Onwuemesi GA, Egboka B, Anudu GK, Omali A (2013) A review of hydrocarbon prospects in the Lower Benue Trough, Nigeria: another insight from potential field study. AAPG Annual Convention and Exhibition, Abstract 90163

Osinowo OO, Taiwo TO (2020) Analysis of high-resolution aeromagnetic (HRAM) data of Lower Benue Trough, Southeastern Nigeria, for hydrocarbon potential evaluation. NRIAG J Astron Geophys 9:350–361

Pawlowski RS (1995) Preferential continuation for potential-field anomaly enhancement. Geophysics 60:390–398

Reeves C (2005) Aeromagnetic surveys: principles, practice and interpretation. Geosoft, Toronto

Reford S (2010) Nigeria's nationwide high resolution airborne geophysical surveys. In: 72nd EAGE Conference and Exhibition, Workshops and Fieldtrips, Barcelona, cp-162-00026. https://doi.org/10.3997/2214-4609.20149924

Reid AB, Allsop JM, Granser H, Millett AJ, Somerton IW (1990) Magnetic interpretation in three dimensions using Euler deconvolution. Geophysics 55:80–91

Reijers TJA, Nwajide CS (1998) Geology of the southern Anambra Basin. In: Reijers TJA (ed) Selected chapters on geology. SPDC, Warri, pp 133–148

Reyment RA (1965) Aspects of the geology of Nigeria. Ibadan University Press, Ibadan

Roberts RL, Hinze WJ, Leap DI (1990) Data enhancement procedures on magnetic data from landfill investigations. In: Ward SH (ed) Geotechnical and environmental geophysics, vol 2. Society of Exploration Geophysicists, Tulsa, pp 261–266

Roest WR, Verhoef J, Pilkington M (1992) Magnetic interpretation using the 3-D analytic signal. Geophysics 57:116–125. https://doi.org/10.1190/1.1443174

Salem A, Williams S, Fairhead JD, Ravat D, Smith R (2007) Tilt-depth method: a simple depth estimation method using first-order magnetic derivatives. Lead Edge 26:1502–1505

Salem A, Williams S, Fairhead JD, Smith R, Ravat D (2008) Interpretation of magnetic data using tilt-angle derivatives. Geophysics 73:L1–L10

Spector A, Grant FS (1970) Statistical models for interpreting aeromagnetic data. Geophysics 35:293–302

Talwani M, Heirtzler JR (1964) Computation of magnetic anomalies caused by two-dimensional structures of arbitrary shape. In: Parks GA (ed) Computers in the mineral industries. Stanford University Publications, Geological Sciences 9, pp 464–480

Talwani M, Worzel JL, Landisman M (1959) Rapid gravity computations for two-dimensional bodies with application to the Mendocino submarine fracture zone. J Geophys Res 64:49–59. https://doi.org/10.1029/JZ064i001p00049

Telford WM, Geldart LP, Sheriff RE (1990) Applied geophysics, 2nd edn. Cambridge University Press, Cambridge

Thompson DT (1982) EULDPH: a new technique for making computer-assisted depth estimates from magnetic data. Geophysics 47:31–37

Thompson R, Oldfield F (1986) Environmental magnetism. Allen and Unwin, London

Ugwu GZ, Ezema PO, Ezeh CC (2013) Interpretation of aeromagnetic data over Okigwe and Afikpo areas of the Lower Benue Trough, Nigeria. Int Res J Geol Min 3:1–8

Ukaegbu VU, Akpabio IO (2009) Geology and stratigraphy of Middle Cretaceous sequences northeast of Afikpo Basin, Lower Benue Trough, Nigeria. Pac J Sci Technol 10:518–527

USGS (n.d.) Nigeria. U.S. Geological Survey, National Minerals Information Center. https://www.usgs.gov/centers/national-minerals-information-center/nigeria. Accessed 8 Oct 2026

Verduzco B, Fairhead JD, Green CM, MacKenzie C (2004) New insights into magnetic derivatives for structural mapping. Lead Edge 23:116–119

Weather Spark (n.d.) Average weather in Okigwe, Nigeria, year round. https://weatherspark.com/y/55000/Average-Weather-in-Okigwe-Nigeria-Year-Round. Accessed 8 Oct 2026

737 Whiteman A (1982) Nigeria: its petroleum geology, resources and potential, vols 1–2. Graham and Trotman,
738 London
739 Yenne EY, Green C, Torvela T (2025) Modelling geologic features and structures in the Middle and Lower
740 Benue Trough of Nigeria from gravity and aeromagnetic data sets. J Afr Earth Sci 231